INFLUENCE OF COLD ROLLING AND SUBSEQUENT ANNEALING PROCESSES ON THE FUNCTIONAL FATIGUE PROPERTIES OF HIGH TEMPERATURE NITIHF SHAPE MEMORY ALLOYS

SOĞUK HADDELEME VE SONRAKİ TAVLAMA İŞLEMLERİNİN YÜKSEK SICAKLIK NİTİHF ŞEKİL HAFIZALI ALAŞIMLARIN FONKSIYONEL YORULMA ÖZELLİKLERİ ÜZERİNDEKİ ETKİSİ

SONER RUMELLİ

PROF. DR BENAT KOÇKAR
Supervisor

Submitted to Graduate School of Science and Engineering of Hacettepe University as a Partial Fulfillment to the Requirements
for the Award of the Degree of Master of Sciences
in Mechanical Engineering.

2022

ABSTRACT

INFLUENCE OF COLD ROLLING AND SUBSEQUENT ANNEALING PROCESSES ON THE FUNCTIONAL FATIGUE PROPERTIES OF HIGH TEMPERATURE NITIHF SHAPE MEMORY ALLOYS

Soner RUMELLİ

Master of Sciences, Department of Mechanical Engineering
Supervisor: PROF. DR BENAT KOÇKAR
May 2022, 70 Pages

Shape memory alloys are very special alloys that can be used as actuators in various applications due to their capability of returning to a prearranged shape via heating under applied load. Their high power per weight ratio makes them an important alternative to conventional pneumatic, hydraulic and motor kind of solid-state heavy actuators, primarily in the aerospace industry. The majority of applications in the aerospace industry demand continuous actuation with transformation temperatures exceeding 100 °C. To judge the feasibility of adopting shape memory alloys in industrial applications, the stability of shape memory properties in terms of actuation strain and transformation temperatures at high temperatures during operational life time is essential. Therefore, shape memory alloys, which have transformation temperatures higher than approximately 100°C, are being widely studied for their utilization in high-temperature applications. Adding hafnium to NiTi binary alloys is one of the most effective ways to create a High Temperature Shape Memory Alloy (HTSMA). HTSMAs undergo thermal, mechanical or thermomechanical treatments to enhance their actuation abilities and stability of shape memory properties and make them a valid option for actuation applications. In this study, the effects of cold rolling with different reduction thicknesses and subsequent annealing conducted at different temperatures on the functional fatigue properties $Ni_{50.1}Ti_{19.9}Hf_{30}$ (at%) were investigated. The material utilized in this work was produced by vacuum

induction melting using high purity Ni, Ti, and Hf elements and the cast billet was hot extruded at 900°C for achieving chemical homogeneity. To analyze the influence of the cold rolling and subsequent annealing on the functional parameters, all of the samples were homogenized to get rid of any texture formation in the material. The first set of samples was cold-rolled by 2% and the second set was cold-rolled by 5%. Then, three samples in each set were annealed at the following different temperatures: 500, 550, and 600 °C. In each set, one sample was kept in cold rolled condition. The transformation temperatures of all samples were first examined by Differential Scanning Calorimetry (DSC). Afterward, the samples with the selected conditions were thermally cycled under 300MPa with a 15°C/sec heating cooling rates to determine the functional fatigue properties such as the evolution of fatigue life, actuation strains, accumulated irrecoverable strains, and transformation temperatures. DSC measurements showed that an increase in cold work percentage reduced the transformation temperatures since cold work led to an increase in dislocation density and thus, suppressed the phase transformation. On the other hand, transformation temperatures increased as the annealing temperature was increased since annealing caused partial annihilation of dislocations, thus reduced dislocation density in the sample. Functional fatigue test results revealed that cold rolling with subsequent annealing stabilized the shape memory parameters and increased the actuation strains since annealing removed the rolling induced dislocation with the internal stress fields in the matrix and increased the amount of transforming volume. However, 30at% of hafnium content made the material extremely hard to deform, and micro-cracks were induced during cold rolling and these micro-cracks were propagated fast during functional fatigue tests and shortened the fatigue lives. Additionally, $Ni_{50.1}Ti_{19.9}Hf_{30}$ (at%) alloy showed very high plastic deformation with 300MPa of loading since full austenite transformations of the alloy can be achieved at approximately 600°C under this stress magnitude.

Keywords: High Temperature Shape Memory Alloys, Functional Fatigue, Cold Rolling, Annealing, Transformation Temperatures, Actuation Strain

ÖZET

SOĞUK HADDELEME VE SONRAKİ TAVLAMA İŞLEMLERİNİN YÜKSEK SICAKLIK NİTİHF ŞEKİL HAFIZALI ALAŞIMLARIN FONKSİYONEL YORULMA ÖZELLİKLERİ ÜZERİNDEKİ ETKİSİ

Soner RUMELLİ

Yüksek Lisans, Makina Mühendisliği Bölümü
Tez Danışmanı: Prof. Dr. Benat KOÇKAR
Mayıs 2022, 70 Sayfa

Şekil hafızalı alaşımlar, yük altında ısıtıldıklarında önceki şekillerini geri kazanabildiği için birçok uygulamalarda aktüatör olarak yararlanılabilen özel malzemelerdir. Ağırlık başına düşen yüksek güç oranları, onları başta havacılık endüstrisi olmak üzere, geleneksel pnömatik, hidrolik ve motor tipi katı hal ağır aktüatör kullanımları yerine kullanılabilecek önemli bir alternatif yapar. Havacılık endüstrisindeki uygulamaların çoğu, eyleyicilerde süreklilik ve 100 °C'yi aşan dönüşüm sıcaklıkları gerektirir. Şekil hafıza özelliklerinin endüstriyel uygulamalarda başarısını belirleyebilmek için, şekil hafızalı alaşımların eyleyici gerinimi ve yüksek dönüşüm sıcaklıklarının görev ömrü boyunca muhafaza edilmesi hayati önem taşımaktadır. Bu nedenlerden ötürü, sıcaklık gereksinimi yüksek uygulamalarda kullanım amacıyla dönüşüm sıcaklığı 100 °C'den yüksek şekil hafızalı alaşımlar üzerine araştırmalar yoğunlaşmıştır. İkili NiTi alaşımına hafniyum eklemek, yüksek sıcaklıklı bir şekil hafızalı alaşım yapmanın en etkili yollarından biridir. Yüksek sıcaklıklı şekil hafızalı alaşımlar, eyleyicilik kabiliyetinin artırılması, şekil hafıza özelliklerinin istikrarını iyileştirmesi ve eyleyici uygulamalarında uygun bir seçenek haline getirilmesi amacıyla termal, mekanik ve termomekanik işlemlere tâbi tutulur. Bu çalışmada, soğuk haddeleme ile farklı kalınlıklara düşürme ve haddelemeye müteakip farklı sıcaklıklarda tavlama yöntemlerinin $Ni_{50.1}Ti_{19.9}Hf_{30}$ (at%) alaşımının fonksiyonel yorulma özellikleri üzerindeki etkileri araştırılmıştır. Bu

çalışmada kullanılan malzeme, oldukça saf Ni, Ti ve Hf elementlerininin vakum indüksiyon eritme prosesi ile üretilmiştir. Kimyasal homojenite sağlamak amacıyla da 900 °C'de sıcak ekstrüde edilmektedir. Soğuk haddeleme ve müteakip tavlamanın fonksiyonel parametreler üzerindeki etkisini analiz etmek ve malzeme içerisinde doku oluşumunu önlemek amacıyla tüm numuneler homojenizasyon işleminden geçirilmiştir. Bir grup numuneye %2'lik, diğer bir gruba ise %5'lik soğuk haddelenme işlemi uygulanarak kalınlıkları azaltılmıştır. Daha sonra gruplardaki numunelerden üçer tanesine 500°C, 550°C ve 600 °C sıcaklıklarda tavlanma işlemi uygulanmış ve birer tanesi tavlanmadan bırakılmıştır. Ayrıca soğuk haddeleme ve tavlama işlemleri yapılmamış bir başlangıç numunesi ayrılmış ve sonuçlar bu numunenin sonuçları ile karşılaştırılmıştır. Diferansiyel Tarama Kalorimetrisi ile tüm numuneler için dönüşüm sıcaklıkları incelenmiştir. Test edilmeye uygun görülen numuneler ile yorulma ömrü, eyleyici gerinimleri, birikmiş plastik gerinimler ve dönüşüm sıcaklıkları gibi fonksiyonel yorulma özelliklerinin tayin edilmesi amacıyla 300MPa yük altında 15 °C/s ısıtma soğutma hızlı ile, termal çevrimler gerçekleştirilmiştir. Diferansiyel taramalı kalorimetri ölçümlerine göre; soğuk haddeleme miktarındaki artış, dönüşüm sıcaklıklarını azaltmıştır. Çünkü soğuk haddeleme dislokasyon yoğunluğunu arttırıp faz dönüşümünü baskılamıştır. Öte yandan tavlama işlemi, dislokasyonları kısmen yok olmasına neden olup numunedeki dislokasyon yoğunluğunu azalttığından, tavlama sıcaklığı yükseltildikçe dönüşüm sıcaklıkları da artmıştır. Fonksiyonel yorulma testi sonuçları; soğuk haddeleme işlemeninden sonra tavlamanın, şekil hafıza parametrelerini kararlı hale getirdiğini ve tavlamanın matristeki haddeleme sonucu oluşan yoğun dislokasyon miktarını ve iç gerilmeleri azaltarak dönüşebilen hacim miktarını arttırdığı için eyleyici gerinimlerinin de arttırdığını ortaya koydu. Bununla birlikte, hafniyum içeriğinin 30at% olması malzemeyi deforme etmeyi son derece zorlaştırması ile soğuk haddeleme sırasında oluşan mikro çatlakların test sırasında hızlı ilerlemesinden dolayı alaşımın fonsiyonel yorulma ömürleri kısalmıştır. Ayrıca $Ni_{50.1}Ti_{19.9}Hf_{30}$ (at%) alaşımında, 300MPa gerilme altında, tam östenit dönüşümünün 600 °C civarında elde edilmesi sebebiyle, bu gerilme altında yüksek plastik deformasyon gözlemlenmiştir.

Anahtar Kelimeler: Yüksek Sıcaklık Şekil Hafızalı Alaşımlar, Fonksiyonel Yorulma, Soğuk Haddeleme, Tavlama, Dönüşüm Sıcaklıkları, Eyleyici Gerinimi

ACKNOWLEDGEMENTS

First and foremost, I would like to express my gratitude to Prof. Benat KOÇKAR for her encouragement, close guidance, and endless patience in my study and especially for her care that showed she was more than a thesis advisor.

This study was supported by the Turkish Aerospace under Grant no. DKTM/2015/10; therefore, I would like to express my sincere gratitude to my company.

I would also like to thank my committee members, Prof. Murat Köksal, Prof. Bora Maviş, Prof. Ziya Esen and Assoc. Prof. Bilsay Sümer for serving as my committee members and also for letting my defense be an enjoyable moment, and for your brilliant comments and suggestions, thanks to you.

I would like to thank everyone in the Hacettepe University Advanced Materials Laboratory for their help and advice, especially Halil Onat Tuğrul and Oğulcan Akgül.

I also thank my division in company for providing academic leave for my master's degree studies. I would like to especially thank Süleyman Kaancan Ataer for motivating me and helping to reduce my workload so that working on my thesis study on work days was possible. And I would like to thank İlteriş Berke Harmancı for his encouragement and support in writing my thesis.

I would like to express my special thanks to my dear wife, Diana Liliana Rumelli, for her support during my studies and also for standing by me during my stressful days.

I would like to thank to my dear cousin Zeki Getizmen for his precious guidance and motivation during my study.

Finally, I would like to express my gratitude to my dear father, İbrahim Rumelli, my mother, Serpil Rumelli, my brother Muti Rumelli, and his wife Meltem Rumelli for their unwavering support, which extends beyond my thesis study.

TABLE OF CONTENTS

LIST OF FIGURES

LIST OF TABLES

SYMBOLS AND ABBREVIATIONS

Symbols

Ni	Nickel
Ti	Titanium
Hf	Hafnium
ε_{mar}	Martensite Strain
ε_{aus}	Austenite Strain
ε_{act}	Actuation Strain
ε_{irr}	İrrecoverable Strain
T_{hys}	Temperature Hysteresis

Abbreviations

A_s	Austenite Start Temperature
A_f	Austenite Finish Temperature
M_s	Martensite Start Temperature
M_f	Martensite Finish Temperature
DSC	Differential Scanning Calorimetry
SMA	Shape Memory Alloy
SMP	Shape Memory Polymer
TT	Transformation Temperature
SME	Shape Memory Effect
FFT	Functional Fatigue Test
WEDM	Wire Electro Discharge Machining
HTSMA	High Temperature Shape Memory Alloy
UCT	Upper Cycle Temperature
ECAE	Equal Channel Angular Extrusion
H	Homogenized
H-CR2	Homogenized-2% Cold Rolled
H-CR5	Homogenized-5% Cold Rolled
H-CR5-An500-30m	Homogenized-5% Cold Rolled-Annealed at 500°C for 30 minutes
H-CR5-An600-30m	Homogenized-5% Cold Rolled-Annealed at 600°C for 30 minute

1. INTRODUCTION

Shape memory alloys (SMAs) are extraordinary materials that can retrieve their original shape after being deformed in the martensite phase and then heated back to the austenite phase. These alloys can recover their shape via heating even under applied stresses and hence they can be used as actuators due to their ability to produce work against load. There are four specific Transformation Temperatures (TTs) at which martensitic and austenitic transformations begin and finish are Martensite Start (M_s), Martensite Finish (M_f), Austenite Start (A_s) and Austenite Finish (A_f). NiTi alloys are the most intensively studied SMAs because of their dimensional and thermal stability. However, the low TTs of NiTi alloys restrain their use at high-temperatures as actuators in aerospace applications. As a result, the tailoring of the TTs has been extensively investigated in the literature, and it has been discovered that TTs of the alloys can be increased by adding a third element or more to NiTi-based SMAs. Hf is favored among the other alloying element alternatives since it is relatively inexpensive and the increase in TTs is very significant with the addition of Hf. NiTiHf High-Temperature Shape Memory Alloys (HTSMAs) have drawn a lot of attention in recent years due to the high operating temperature requirements in aerospace and automotive applications [1].

Actuator stability is strongly desired in aerospace applications. Thus, the fatigue life of HTSMAs must be evaluated for the lifetime design of actuators since alloys can lose their shape-recovery capability with the number of actuation cycles at high temperatures due to the formation of plastic deformation under applied stress and with phase transformation via heating and cooling. To tackle with this problem, thermal, mechanical and thermo-mechanical treatments that result changes in the microstructure can be applied to SMAs For example, plastic deformation methods produce high dislocation density and fine deformation twins, which lead to an increase in critical shear stress for slip and hence shape memory properties and cyclic stability of the alloys can be enhanced [2].

SMAs have been extensively examined in terms of their response to severe plastic deformation (SPD) and conventional deformation methods. In equiatomic NiTi alloys, cold working causes dislocations in the material, which brings martensite stabilization and decrease in TTs. Furthermore, in thermal cycling trials, grain size reduction

minimizes residual strain and an increase in resistance to dislocation slip which results to observe cyclic stability [3].

SPD induces high dislocation densities and leads to produce very fine grains in the SMA, and generally, subsequent annealing heat treatment is applied for better SMA properties. Annealing of SMAs is proven to be an efficient way to alter the SMA properties with an appropriate heat treatment temperature, heat treatment time, and cooling rate after heat treatment [4]. Studies in the literature show the effect of reduced grain size and a corresponding increase in grain boundary area on the shift in transformation temperatures. It is shown that grain boundaries and dislocations act as barriers to martensite-austenite transformation and increasing grain boundary area and the dislocation density suppresses the phase transformation [5]. Due to this reason, actuation strain decreases. Heat treatment helps to reverse these plastic deformation effects with the annihilation of excess dislocations, which enhance actuation abilities of the alloys [6].

Although there have been studies on Hf-added NiTi alloys, no studies have been conducted regarding the effect of thermo-mechanical operations on the functional properties of NiTiHf alloys containing 30% (at%) hafnium. In this study, functional properties of $Ni_{50.1}Ti_{19.9}Hf_{30}$ (at%) and the effect of cold-rolling with subsequent annealing were examined for the first time up to author's best knowledge. The functional properties such as actuation strains, irrecoverable strains, thermal hysteresis, and TTs were determined with the cooling-heating cycles under 300 MPa constant stress magnitudes. To analyze the influence of the cold-rolling and subsequent annealing on the functional properties, all samples were homogenized to get rid of any directional dependency due to hot extrusion process, which was conducted after casting, in the material. The first set of samples was cold-rolled by 2% and the second set was cold-rolled by 5%. Then, three samples in each set were annealed at following temperatures: 500, 550, and 600 °C. In each set, one sample was kept as it was and no annealing was conducted. Firstly, TTs of all samples were examined via using Differential Scanning Calorimetry (DSC) (Perkin Elmer 8000) and some of them were chosen depending on the change in TTs for functional fatigue experiments.

For the sake of simplicity, some abbreviations were used for the samples that were exposed to thermomechanical treatments. Homogenized samples were presented with the letter “H”, cold-rolled were presented as “CR” and annealed samples were presented with the letters “An”. The percentage of the cold rolling, the annealing temperatures and the duration of the annealing time were added to the end of the abbreviations. For example, H-CR5-An500-30m sample was the one which was first homogenized, then cold-rolled by 5% reduction in thickness, and finally annealed at 500 °C for 30 minutes.

2. THEORY AND LITERATURE

Nitinol (NiTi) was developed by the U.S. Naval Ordnance Lab early in the 1960s [7]. The shape memory phenomenon was demonstrated at an international symposium in Toronto in 1975 by investigators with diverse metallurgical interests, and the number of patents on SMAs has steadily increased until today, and the investigations reported in 1979 [8]. SMAs are special alloys that can regain their predetermined shape after being deformed in their low-temperature martensite phase and then heated back to their austenite phase. This phenomenon is called the "Shape Memory Effect (SME)". There is another effect, which is called "Superelasticity" (SE). SMA is loaded to a relatively high strain magnitude (higher than elastic strain), and when it is unloaded, it gets back to its original shape. For the SE behavior the alloy should be loaded while it is kept in its austenite phase. SMAs have many application areas in health, automotive, and aviation industries because of their SME and SE abilities [1].

The SME behavior is described schematically in Figure 2.1-1. The alloy is at its high-temperature phase at point 1, which is called austenite. Then, it is cooled down from point 1 to 2 and, by cooling, the material transforms into twinned martensite. There is no shape change occurring during this cooling. The alloy is loaded as it is shown from point 2 to 3 without a change in temperature. During this loading, the twinned martensite structure transforms to detwinned martensite as shown in Figure 2.1-1 and the shape change is observed. The material with the detwinned structure is unloaded following the route from points 3 to 4. To recover the shape change, the material is heated back to austenite phase. So, the detwinned martensite is transformed to austenite via heating through the route 4 to 1 and the shape recovery is achieved. The superelasticity effect is also shown in Figure 2.1-1. At point 1, the material is in its austenite phase. When loaded (1 to 2), the alloy elastically deforms and then starting from point 2 it begins to transform into twinned martensite structure. Further loading results in the transformation of twinned martensite into a detwinned martensite structure. After the material is unloaded from point 3, the elastic recovery takes place from point 3 to 4 and then the detwinned martensite transforms to austenite from point 4 to 1. Total removal of the load leads the alloy to go back to its original shape and structure.

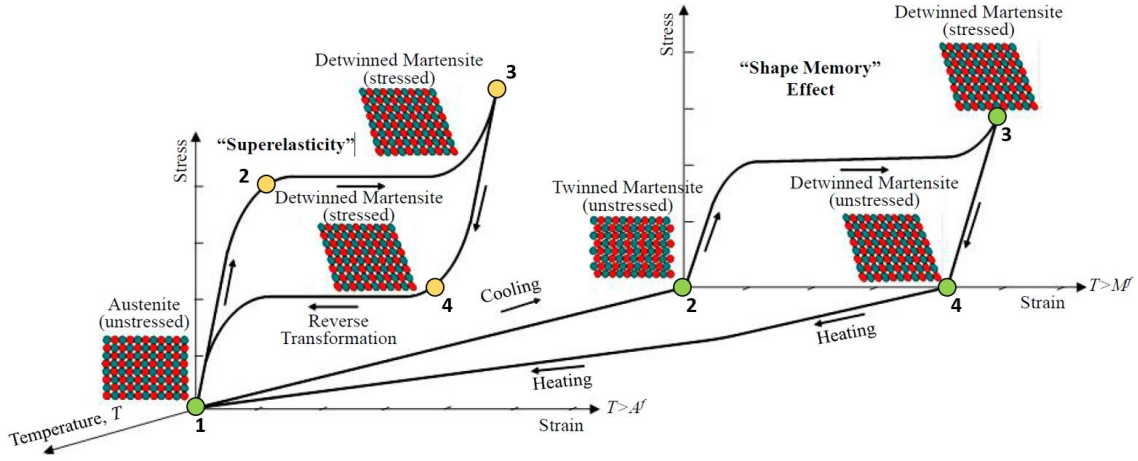

Figure 2.1-1. Illustration of SME and SE [9].

The SME and the SE mechanisms that were explained above make them very useful in specific applications. There are numerous applications of SMAs in different areas for more than four decades. SMAs have been already commercialized in medical applications. For instance, the most popular SMA application in the medical area is the production of stents from these alloys. Usage of a balloon to enlarge the arteries is replaced by a self-expanding SMA device to open the blocked passages. SMA stent is inserted into the artery and it recovers its expanded shape at body temperature. Predefined self-expansion helps to avoid over-expanding and possible injuries of the veins [10].

SMAs are commonly utilized in the aerospace area. The wings of the planes are morphed using SMA-based actuators. NiTi alloy wires are pre-stressed and placed into a Kevlar/Epoxy composite. Pre-stressed NiTi wires helps tailoring natural vibration frequencies to the required design range [11]. Brailowski et al. [12] used a “coupled thermo-mechanical approach” to model morphing wings and validated the results in tunnel tests. According to their results, using SMAs improved fuel economy by altering the shape of the wings with the air flow regime such that the friction can be minimized. SMAs are also used in aircraft flaps. The flaps can be actuated using SMA plates or wires via heating and cooling. These are called "smart" or "adaptive" wings [13]. Cooling can be achieved naturally due to very low temperatures at higher altitudes but cooling rate should be controlled since the flight velocity is very high and always changes.

SMAs have a great potential for overcoming various unusual difficulties in space missions. They can be used in actuation and release mechanisms and vibration dampers during launch of the space vehicle to a hard surface in space. Micro-vibrations produced in the space bus are the main concern during taking high-resolution quality images. Kwon et al. [14] proposed "Pseudoelastic SMA Mesh Washers" as a solution to this problem. The large hysteresis and high non-linearity features of SMAs are used to successfully separate these micro-vibrations via adding or removing loads. The usage of SMA in the production of hinges enhances solar array deployment technologies as well [15]. The SMA not only decreases the cost of the system and increases its reliability, but also reduces shocks in the release mechanisms and enhances spaceship kinematics. The separation of the spacecraft before the launch was improved years ago by Johnson's Patent on SMA release system [16]. Johnson suggested a schockless release mechanism in which the SMA is loaded in the martensitic phase and then it is heated to regain its initial shape and phase. This application helps to separate spacecraft without any shock to the spacecraft.

As explained above, SMAs are utilized extensively and have characteristic features. To characterize the SMAs to be useful for a specific application, some parameters such as transformation temperatures (TTs), irrecoverable or plastic strain, temperature hysteresis, actuation or working strain are required to be investigated to decide whether the SMA is usable for the task or not. These parameters are shown in the strain-temperature graph in Figure 2.1-2 for an SMA when it is heated and cooled under applied constant stress. The blue line shows the change in strain while cooling the alloy down to martensite phase, and the red line shows the change in strain while heating the alloy to its austenite phase. The strain that material shows when it is in the martensite phase is called the martensite strain (ε_{mar}), and the strain that material shows in the austenite phase is called the austenite strain (ε_{aus}). The strain difference between the material's martensite strain and the austenite strain is called the actuation strain (ε_{act}) and the strain difference between the austenite strain of the initial a cycle and the austenite strain of the next cycle is called as irrecoverable strain (ε_{irr}). The summation of the irrecoverable strain and the actuation strain is defined as the transformation strain.

Phase transformation temperatures can simply be obtained by drawing tangent lines to these heating and cooling curves. Austenite start (A_s) and finish (A_f) temperatures may be attained by reading the intersections of tangent lines to the heating curve, whereas martensite start (M_s) and finish (M_f) temperatures can be determined via reading the temperatures at the intersections of tangent lines of the cooling curve in the same way. Finally, temperature hysteresis (T_{hys}) can be obtained by reading the temperature difference between the mid points of the heating and cooling curves.

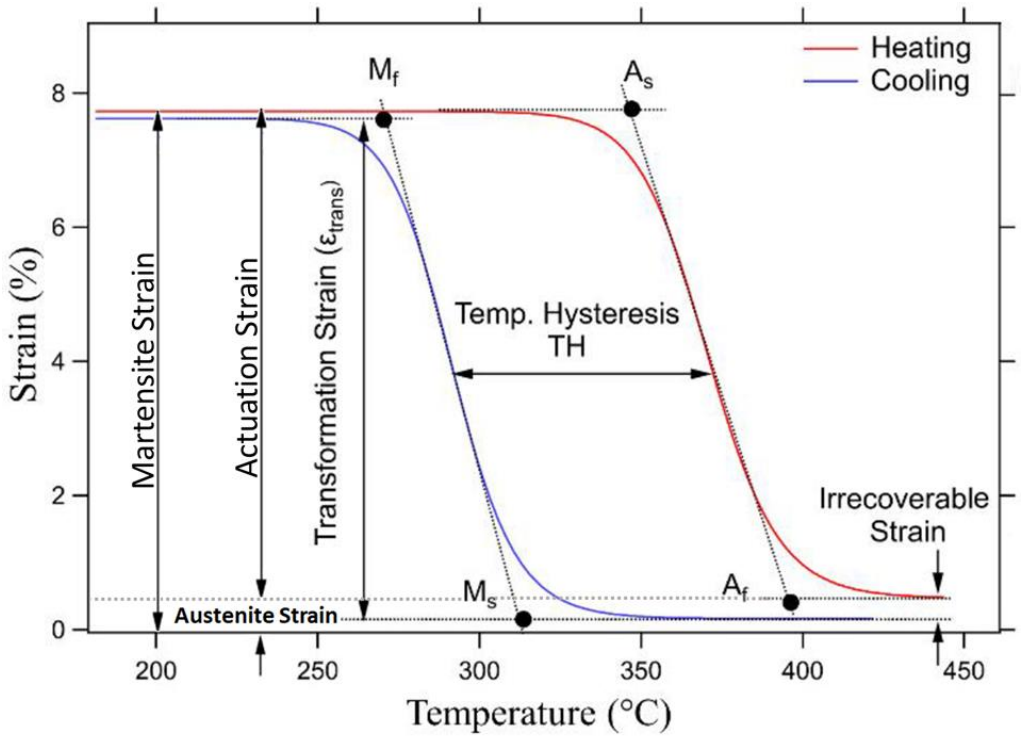

Figure 2.1-2. Strain-Temperature curve of SMAs while heating and cooling [17].

The principle of the SMAs being used as actuators is explained in Seelecke's review article [1] with a simple example. Seelecke describes a typical NiTiCu-SMA actuator ribbon works under load of 0.01 kN. The ribbon is extended while the alloy is in its martensite phase and then heated to A_s temperature to achieve shrinkage. The ribbon shrinks entirely at A_f temperature. In the case of cooling, on the other hand, a hysteresis loop is observed, with an extension not initiating until martensite reaches M_s temperature. Stretching continues until the temperature is decreased down to M_f. This SMA can be utilized as an actuator because of the strain achieved through stretching and recovering the strain via heating loop as shown in Figure 2.1-3.

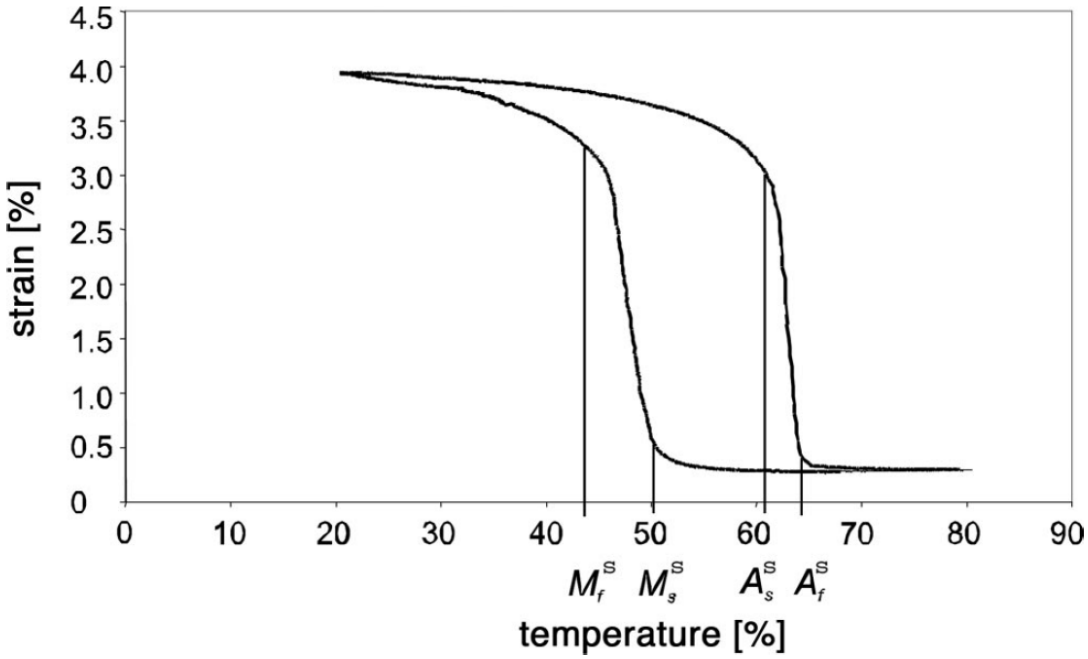

Figure 2.1-3. Deformation vs Temperature curve of a typical NiTiCu wire [1].

2.1. Functional Fatigue of NiTi-SMAs

In industrial applications, the reliability and the robustness of the parts are inevitable necessities. Hence, the fatigue life of SMA needs to be investigated. Two kind of fatigue exists in SMAs: "structural fatigue" and "functional fatigue (FF)". When any structural materials are subjected to severe repeated stress and crack initiation/propagation and the decrease the load bearing capacity of the material take place with the number of cycles. Therefore, structural fatigue occurs. The degradation of functional shape memory properties with the number of cooling-heating cycles under applied stress amplitude or the number of loading-unloading cycles owing to microstructure evolution is referred to as Functional Fatigue (FF). FF is related to a rise in residual strain, which occurs as a result of incomplete reverse transformation [18].

Frenzel [19] states that FF implies the deterioration of certain functional-properties such as “actuator stroke, recoverable strain, plateau stresses, hysteresis width, or transformation temperatures”, which occurs as a result of the accumulation of “transformation-induced defects” in the microstructure. Stress amplitude, the volume of transformation, alloy composition, surface polish, and heat treatments are all investigated in the literature as factors impacting FF life. Functional stability of SMAs, on the other

hand, can be increased by increasing the material's resistance to slip, which improves the fatigue resistance.

Babacan [20] studied the thermo-mechanical stability of Cu-Al-Mn SMA alloy for actuator applications by heating the samples to different Upper Cycle Temperatures (UCTs) via conducting stress-free thermal cycling and also under constant stress heating-cooling experiments by setting several UCTs. Stress was discovered to be an activating factor for bainitic transformation at the UCT and during holding time at UCTs. Moreover, the shift of TTs changes with the change of UCTs. Dislocation generation, ordering of the parent phase, and dominance of bainitic transformation were found to be reasons for the increase in the TTs. Karakoc et al. [21] explored the cyclic stability and FF life of the nickel-rich $Ni_{50.3}Ti_{29.7}Hf_{20}$ alloy as a function of UCT and applied stress. The results of FFTs have shown that increasing UCT and a stress resulted a reduction in the fatigue life [22]. Furthermore, it was shown in another study that the aging at 550 °C for 3 hours enhanced FF life by three times due to the development of nano-precipitates [23].

2.2. Shape Memory Alloys (SMAs)

The research on SMAs has been increasing over the last few years due to the interest in using them as actuators. Smaller size with lower weight of SMAs compared to “pneumatic, hydraulic, and solenoid actuator systems” lead them to be preferred for actuator applications [24]. Since 1960s, Nitinol (NiTi) which is the most frequently used SMA, has ushered in a new era in the usage of active materials with massive recoverable shape changes at high actuation forces. NiTi alloys having different Ni content are being investigated. Ni-rich Ni-Ti is ideal for biomedical applications because of its superior corrosion resistance and its transforming temperatures which are around body temperature. However, the operating temperatures of all NiTi-alloys which are less than 100°C make them unsuitable for high temperature applications [25]. As a result, numerous investigations have been carried out to customize their TTs and other functional features.

SMA's functional qualities are greatly influenced by its “composition, grain size, heat treatment history, and loading conditions” [26]. Additional alloying elements in the composition have a big impact on the SMA characteristics. When a scarce percentage of

copper is added to NiTi-SMA, the TTs become insensitive to composition and the thermal-hysteresis difference mitigates [27]. Addition of small amount of palladium increases the TTs above 200 °C [28].

Other than NiTi-based SMAs, Cu and Fe-based alloys are also being studied due to their low-cost advantage. Fe-based-SMAs are preferred since they have better SE properties at low temperatures, and the most commonly used Fe-based-SMAs are "Fe-Ni-Co-Ti, Fe-Pt, and Fe-Pd" [29]. Cu-based SMAs are relatively inexpensive, and they can be designed to operate at higher temperatures by using ternary-alloys like "Cu-Zn-Al and Cu-Al-Mn", which have higher TTs [30]. Even though Cu-based SMAs have higher ductility, their limited resistance to grain boundary fracture makes them unsuitable for actuator applications [31].

2.2.1. High Temperature Shape Memory Alloys (HTSMAs)

Although binary NiTi SMAs are widely used in commercial applications, their operating temperature range prevents them from being used in high-temperature applications in aerospace and automotive industries. As a result, HTSMAs, which are defined as alloys with an austenite start (A_s) temperature approximately greater than 120 °C in stress-free conditions [32], have been developed. Their thermomechanical properties, such as TTs and transformation strains, have been improved, allowing them to be utilized as actuators in high temperature applications.

There is strong desire to have HTSMAs, which exhibit "long-term stability, resistance to plastic deformation and creep, and adequate environmental coherency". Because of the ordered intermetallic crystalline structure of these materials, these criteria become more onerous as working temperatures rise. However, studies reveal that adjusting the composition and applying a series of subsequent thermomechanical operations can help to overcome these challenges [33].

The addition of Pd, Pt, Zr, Au, or Hf as ternary elements is frequently studied in the literature. As a ternary element, Zr has a relatively low cost. On the other hand, their thermal hysteresis is larger, and Zr makes the alloy brittle due to its high oxygen affinity. Au, Pt, and Pd increase the cost significantly, which makes them not feasible for using as

the additional alloying element [34]. Therefore, interest in Hf as a ternary element in NiTi-based SMAs has increased lately for HTSMA production due to relatively lower costs and higher work outputs as shown in Figure 2.2-1.

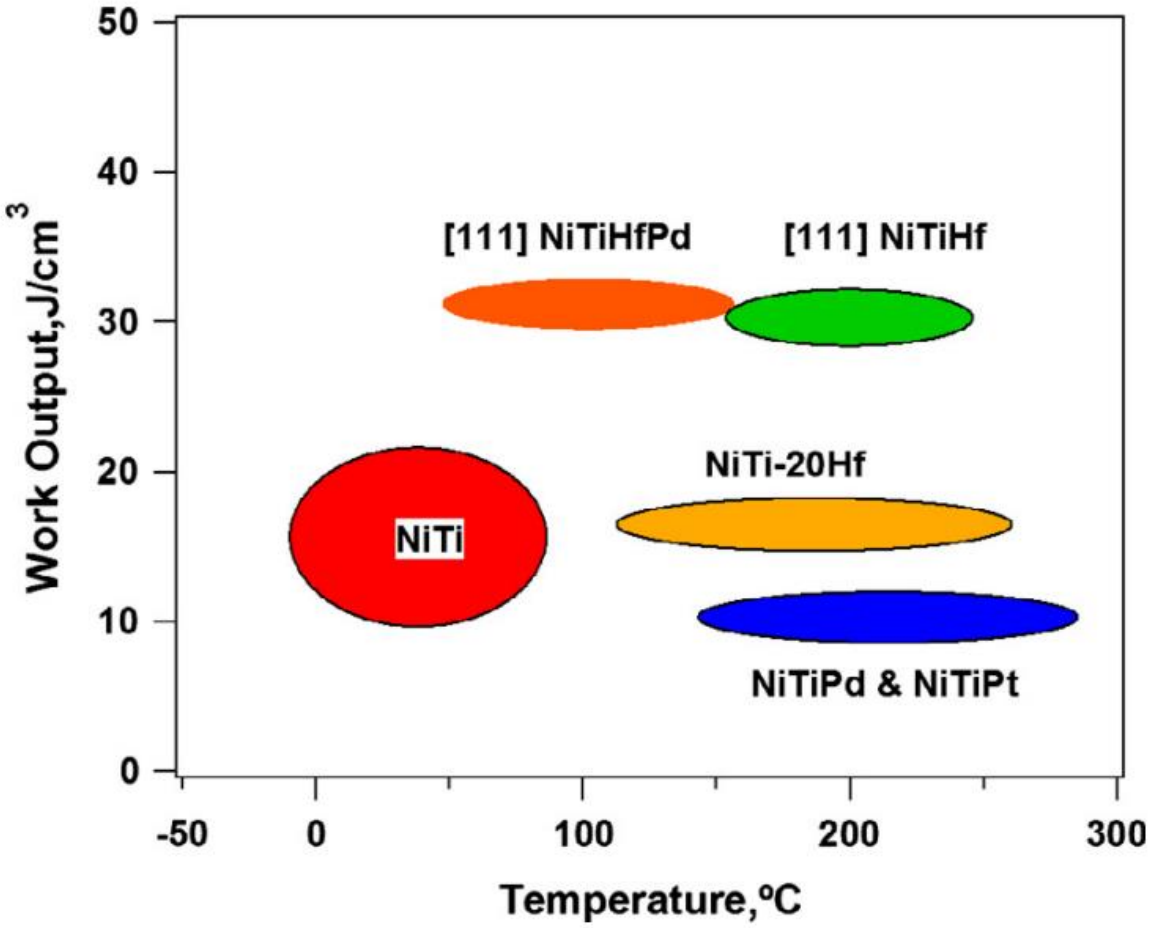

Figure 2.2-1. Work output comparison of NiTi-based SMAs [35].

2.2.2. NiTiHf-HTSMA

Because of their low cost, high TTs, and high work outputs, NiTiHf alloys are intensively researched HTSMAs. Thus, interest in $Ni_{50}Ti_{(50-x)}Hf_x$ alloys has grown, as the interest in HTSMAs intensifies.

Firstly, Potapov et al. investigated Ni-lean NiTiHf-HTSMAs and focused on the effect of the atomic weight percentage of Hf on TTs. As the Hf content increases from 8 (at%) to 20 (at%), the TTs are increased from 50°C-142°C to 127°C-276°C, respectively [36].

Saghaian et al. studies revealed that in Ni-Rich NiTi-20Hf alloys, H-phase precipitate formation leads to a decrease in Ni-content in the matrix and thus the TTs increase [37].

Ni-lean NiTiHf, HTSMAs have relatively high-temperature hysteresis. Furthermore, its cyclic stability is weak because of the high stress required for detwinning and martensite reorientation. Due to their limited ductility, they are very difficult to deform as well. On the other hand, to improve their critical shear strength for slip, NiTiHf alloys undergo severe plastic deformation processes, that improve their cyclic stability and working parameters, such as stabilizing ε_{act} , decreasing ε_{irr} , and also T_{hys} under constant stress [38].

According to studies, increasing the composition of Hf and decreasing Ti content in NiTiHf alloy has no significant effect on TTs until the alloy includes 10% Hf. On the other hand, TTs increase linearly with the increase of Hf content and reach to 525°C with 30 at% of Hf addition. For Ni-lean NiTiHf SMAs, the Ni concentration in the alloy has no significant effect on TTs. However, TTs drop considerably as the alloy's Ni concentration rises above 50 (at%) [39]. Karaca [40] studied the influence of Ni&Hf content to the martensite peak temperatures (M_p). The change in M_p was studied for $Ni_xTi_{90-x}Hf_{10}$ and $Ni_{49}Ti_{51-x}Hf_x$ SMAs as shown in Figure 2.2-2 (a) and (b) respectively. M_p did not change until 50 (at%) of Ni addition to the composition. On the other hand, M_p decreased to below 0 °C dramatically after 50 (at%) of Ni content in the composition as shown in Figure 2.2-2 (a). M_p is unaffected below 3 (at%) of Hf content. M_p gradually increased between 3-10 (at%) of Hf content. However, the change rate of M_p starts to increase after 10 (at%) of Hf content in the composition as shown in Figure 2.2-2 (b).

The shape memory properties of NiTiHf SMAs need to be improved for their actuation capabilities. Aside from changing the alloy composition, other thermomechanical treatments, such as heat treatments and severe-plastic-deformation procedures, can be applied for enhancing actuation properties of SMA.

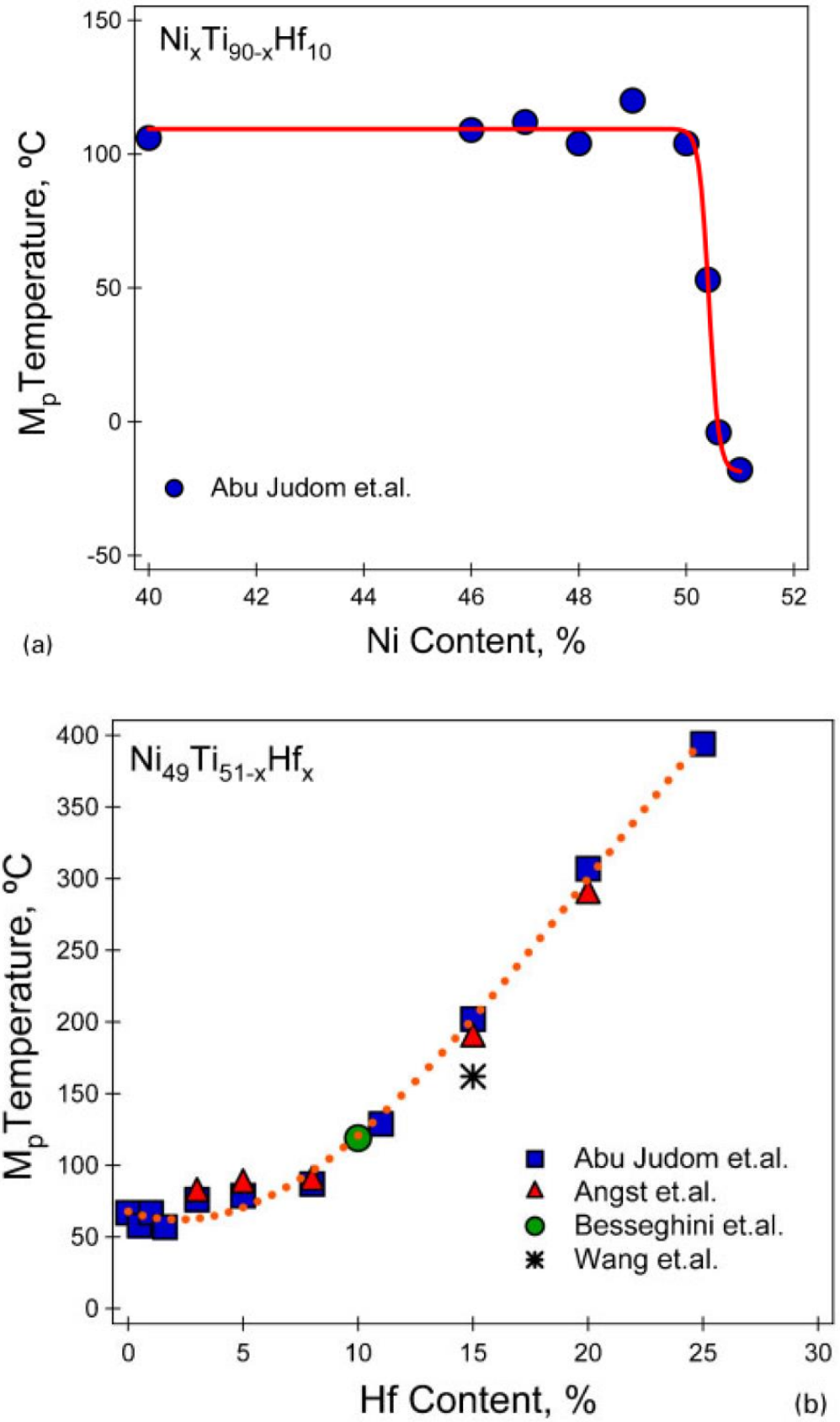

Figure 2.2-2.(a) Mp temperature evolution with Ni content. (b) Mp temperature evolution with, Hf content [40].

2.3. Effect of Mechanical and Thermomechanical Treatments on SMA Properties

Mechanical and thermomechanical treatments are useful to tailor the SMA properties. Mechanical treatments include “refinement of the grain size of the material and the introduction of local internal stresses” which affect the functional parameters of the SMAs [41]. Thermomechanical treatments are mechanical treatments combined with heat treatments. They can help increase cyclic stability by altering the dislocation density in the matrix. In addition, thermomechanical treatments help tailor the functional parameters of the SMAs by altering grain size and grain structure, causing a change in the mobility of the dislocations and strength of the material.

2.3.1. Effect of Plastic Deformation on SMA Properties

High dislocation densities and deformation twins are induced and fine grains can be obtained with plastic deformation processes, which especially enhance “the cyclic stability of the shape memory properties” and increase the fatigue life of SMAs [2]. However, the alloy may become very brittle due to the tremendous increase in dislocation density since deforms plastically, and heat treatment following the plastic deformations can recover the effects of huge plastic deformations such as annihilation of some dislocation forests. The mechanical characteristics of SMAs can be improved via conducting short term annealing after plastic deformation processes [42].

Cold working causes dislocations and some point defects in the matrix that stabilizes martensite in NiTi alloys. The relation between TTs and lattice defects caused by cold working has been demonstrated in the literature [43]. Wu et al. investigated how lattice defects produce internal stresses that shift martensitic transformation to lower temperatures [4]. Generally speaking, the dislocations and the defects pin the martensite-austenite boundary and therefore, it becomes necessary to undercool the alloy to observe martensite formation. The plastic deformation mechanisms and microstructural evolution of CuZnAl SMA were investigated by Adachi et al. [44]. According to the study, the material undergoes variant-variant joining, internal twinning, and slip and stress-induced martensite to martensite transformation when subjected to moderate-intensity cold working.

Pattabi [45] investigated the “effects of cold working and subsequent annealing on the NiTi alloy”. According to this research, increasing the cold working rate caused the disappearance of SME since dislocation forest forms. After annealing at 300 °C, memory effect was restored.

Besides conventional plastic deformation methods, severe plastic deformation (SPD) methods are also carried out in the literature to improve SMA properties. SPD induces high dislocation densities and very fine grains in SMAs and subsequent heat treatment is usually required to improve SMA characteristics. Waitz et al. [46] showed that reducing grain size below 150 nm caused martensitic transformation to occur at a lower temperature because an amorphous structure was formed with High Pressure Torsion (HPT) method at room temperature. Since HPT caused the alloy to lose its shape recovery properties due to the huge decrease in TTs, subsequent annealing above 300 °C was necessary to be applied to recover the shape recovery abilities.

Another way to decrease the grain size is by applying surface mechanical attrition treatment (SMAT). In this technique, a nanostructured surface layer is generated by applying SPD to the surface of the material. Mei et al. [47] studied the effect of SMAT on NiTi SMAs and observed coarse-grained austenite phase (B2 phase) turned into near-uniaxial B2 nanograins on the surface. Stress-induced martensite transformation stress increases as the grain size of nanograins decreases, which means stress-induced martensite formation was suppressed within nanograins.

Influence of the equal channel angular extrusion (ECAE) on $Ti_{50.3}Ni_{33.7}Pd_{16.}$ was investigated by Kockar et al. [48]. According to this study, the microstructure was refined in terms of grain and twin size, and TT and dimensional stabilities were improved after ECAE owing to microstructural refinement, which increases the critical stress for slip. The refinement in microstructural features resulted in a large drop in irrecoverable stresses, and the transformation strain decreased due to the reduction in transformation volume. Because of the smaller grain size, the TTs were also reduced.

2.3.2. Effect of Plastic Deformation with Subsequent Heat Treatment on SMA Properties

Heat treatment of SMAs is a reasonably inexpensive procedure that is effective in changing SMA properties. The effect depends on the "heat treatment temperature, time, and cooling rate of the heat treatment" [4]. The answer to the question of whether the chosen heat treatment is adequate for the alloy or not relies on the basics of the annealing processes.

The annealing process and its stages are explained in Callister's book [49]. Plastic deformation induces dislocations to the material. This plastic deformation causes tensile, compressive, and shear zones in the material; and it is possible to revert these effects by annealing. Annealing has three stages: recovery, recrystallization, and grain growth, which are shown in Figure 2.3-1. During the recovery stage, atomic diffusion increases, and the internal strain energy storage inside of the material is released by the dislocation motion. Some dislocations are annihilated during this motion, and lattice defects decrease. The recrystallization takes place above 0.4–0.7 of the melting temperature of the alloy. In the recrystallization phase, new, equiaxed, strain-free grains start to nucleate. Dislocation densities reduce sharply, while mechanical properties recover almost to the pre-cold working situation if the alloy is held at high temperatures for relatively longer time. The amount of recrystallization depends on temperature and time. In the last stage, grain growth occurs due to further waiting at high temperatures after recrystallization completes. As strain-free grains grow, grain boundary areas decrease, thus, strength decreases, and ductility increases, as shown in Figure 2.3-1.

The arrangement of the dislocations, lattice defects together with the grain size evolution alter transformation properties since dislocations and grain boundaries act as barriers to austenite-martensite boundary mobility, and increasing grain boundary area and dislocation density suppresses the phase transformation [5]. Annealing assists the annihilation of dislocations and point defects, hence, martensite transforming volume boosts [6].

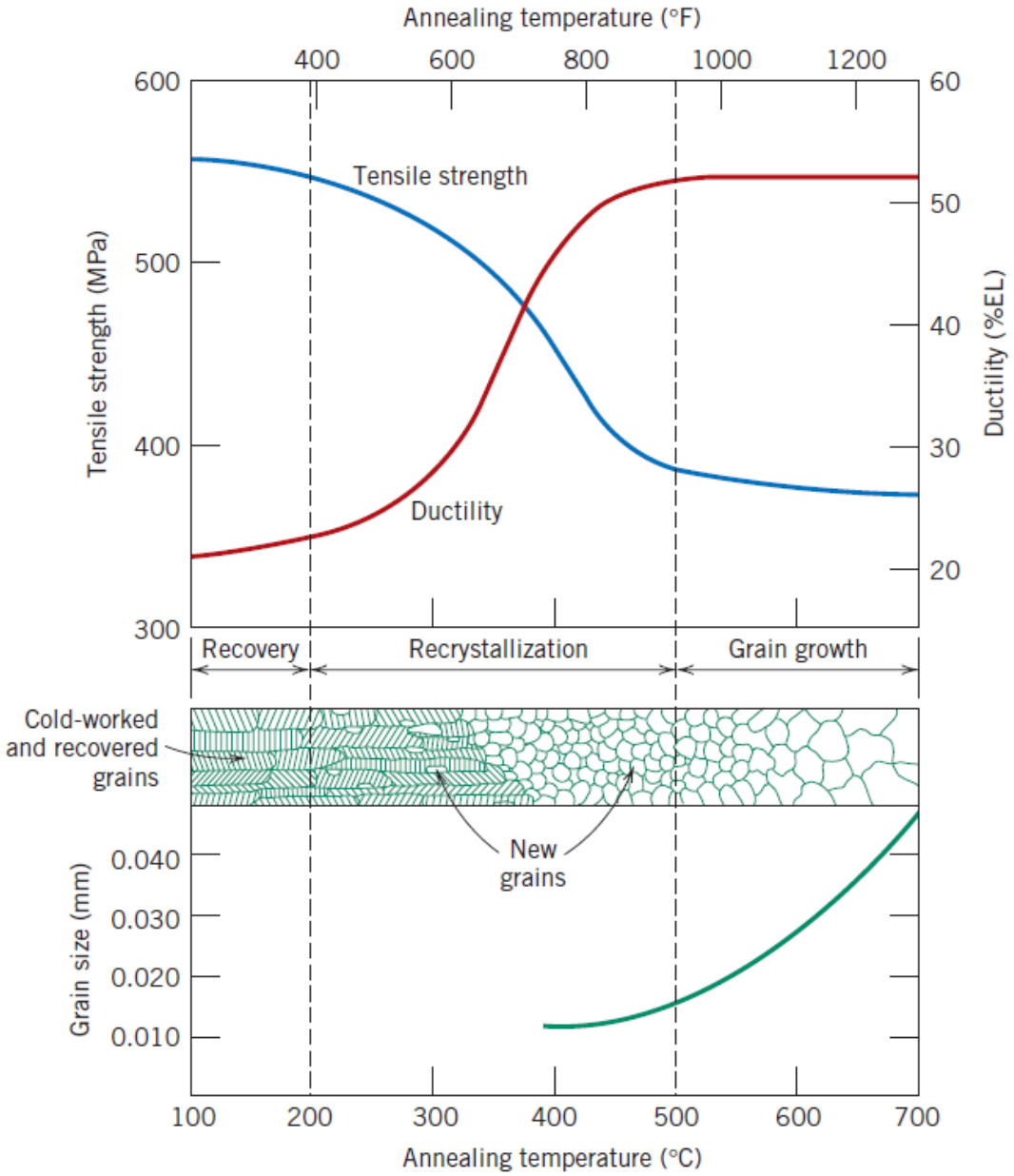

Figure 2.3-1. Illustration of recrystallization processes in elevated temperatures [49].

Babacan et al. [50] investigated the effect of cold-rolling and subsequent annealing on $Cu_{73}Al_{16}Mn_{11}$ (at%). It was found that the effect of refining grains or increasing the grain boundary area suppressed the austenite to martensite transformation. The cold-rolled failed earlier during cooling-heating cycles due to the relatively higher internal stress which was induced via cold rolling. Another sample was cold rolled with a high reduction in thickness and then annealed above the recrystallization temperature. The most successful grain size reduction was attained in this sample. It was found that grain refinement significantly increases the strength of the material. However, it did not

improve superelastic strain. On the other hand, samples having finer grains showed better dimensional stability under constant stress heating-cooling experiments.

Denowh et. al. [51] studied on NiTiHf-SMAs and showed how heat treatment enhances actuation strain with the application of the optimum heat treatment temperature. $(TiHf)_2$ intermetallic which was formed during the heat treatment at relatively higher temperature led a reduction in actuation strain and FF life due to creep effects.

Lagoudas et al. [52] investigated the influence of cold-rolling followed by annealing on $Ni_{50}Ti_{40}Cu_{10}$ SMA. The microstructure did not change considerably at relatively lower annealing temperatures (below 450 °C), and the TTs did not change as well. The partial removal of dislocations in the material caused a shift in TTs to higher temperatures in samples that were annealed at intermediate temperatures (450–550 °C). When the samples were annealed over 600 °C, the effects of recrystallization occurred. In addition, this practice showed the influence of heat treatment temperature on fatigue life. Because the annealing temperature was insufficient for eliminating dislocations, and induced stress localization, samples annealed at lower temperatures had a shorter fatigue life. The partial elimination of dislocations during intermediate temperature annealing led to achieve extended fatigue life. Due to higher recrystallization, which brought the samples to pre-cold working conditions, high-temperature annealed samples had a shorter fatigue life. The study also includes investigation of transformation strains. There is no appreciable increase at lower and moderate annealing temperatures. However, at high annealing temperatures, a reduction in transformation strain was observed. The reason was that the accumulated plastic strain remained in the matrix even though the texture due to cold work had disappeared.

Jiang et al. [42] investigated the microstructural evolution and phase change of NiTi SMAs that had been severely plastically deformed and annealed. Non-homogeneous SPD created amorphous bands with various defects such as stacking faults, dislocations, and twins in the alloy. Amorphous samples were nanocrystallized after 2 hours of annealing at 300 and 450 °C, and these nanocrystalline grains grew as the annealing temperature rose. Annealing at 600°C led to complete crystallization and annealing twins were determined after annealing at 600 °C. Annealing at 300 °C did not create enough thermal

driving force to eradicate dislocation faults in amorphous band structure. As annealing temperature rose grain size increased and, thus, grain boundary area reduced. As a result of this, martensitic phase transformation became favorable than that of the samples having nanocrystalline grains.

Meng et al. [53] studied "the phase change and mechanical characteristics of ultra-thin NiTi sheets" that had been cold-rolled and annealed. Cold rolling caused large internal stresses in the material, which were then reduced by annealing, and led to observe more homogeneous microstructures and lower martensitic transformation temperatures. Gubicza et al. [54] found that annealing at moderate temperatures improved ductility while sacrificing strength by removing dislocations from the CuAlZn SMA. Furthermore, dislocations were reorganized and caused improvement in the shape memory properties.

Apart from annealing, the effect of aging heat treatment has been extensively researched in the literature, since aging produces "H-phase precipitates in Ni-rich NiTiHf SMAs", which reinforce the alloy and improve cyclic stability [55].

Considering both TTs and ε_{act}, Saygili [56] indicated that aging has a favorable influence on the cyclic-stability. In addition, the accumulation of dislocations during transformation cycles under constant load resulted in a dramatic increase in TTs and a considerable reduction in ε_{act} values for the specimen that was not age-hardened. The "thermal and thermo-mechanical stability" of these alloys was damaged with the increase in dislocation amount during cooling-heating cycles. After aging, however, cyclic stability was improved.

Karakoc et al. [21] tested the cyclic stability and FF life of the "Ni-Rich $Ni_{50.3}Ti_{29.7}Hf_{20}$ (at%) alloy" depending on UCT and applied stress. During the FF experiment, it was discovered that increasing UCT and applying stress resulted in a reduction in the FF life. Furthermore, since nano-precipitates form, "aging at 550 °C for 3 hours" enhanced FF life by three times.

3. EXPERIMENTAL PROCEDURE

This work aimed to survey the influence of cold-rolling and subsequent annealing processes on the FF properties of high-temperature $Ni_{50.1}Ti_{19.9}Hf_{30}$ (at%) SMAs. To accomplish this, several samples were prepared and divided into groups based on the thermomechanical treatments which were conducted. Samples were cold-rolled then annealed at various temperatures and compared with the non-treated sample. Processes and experiments that were done on the samples are shown as a flow chart in Figure 2.3-1 and are explained in this section.

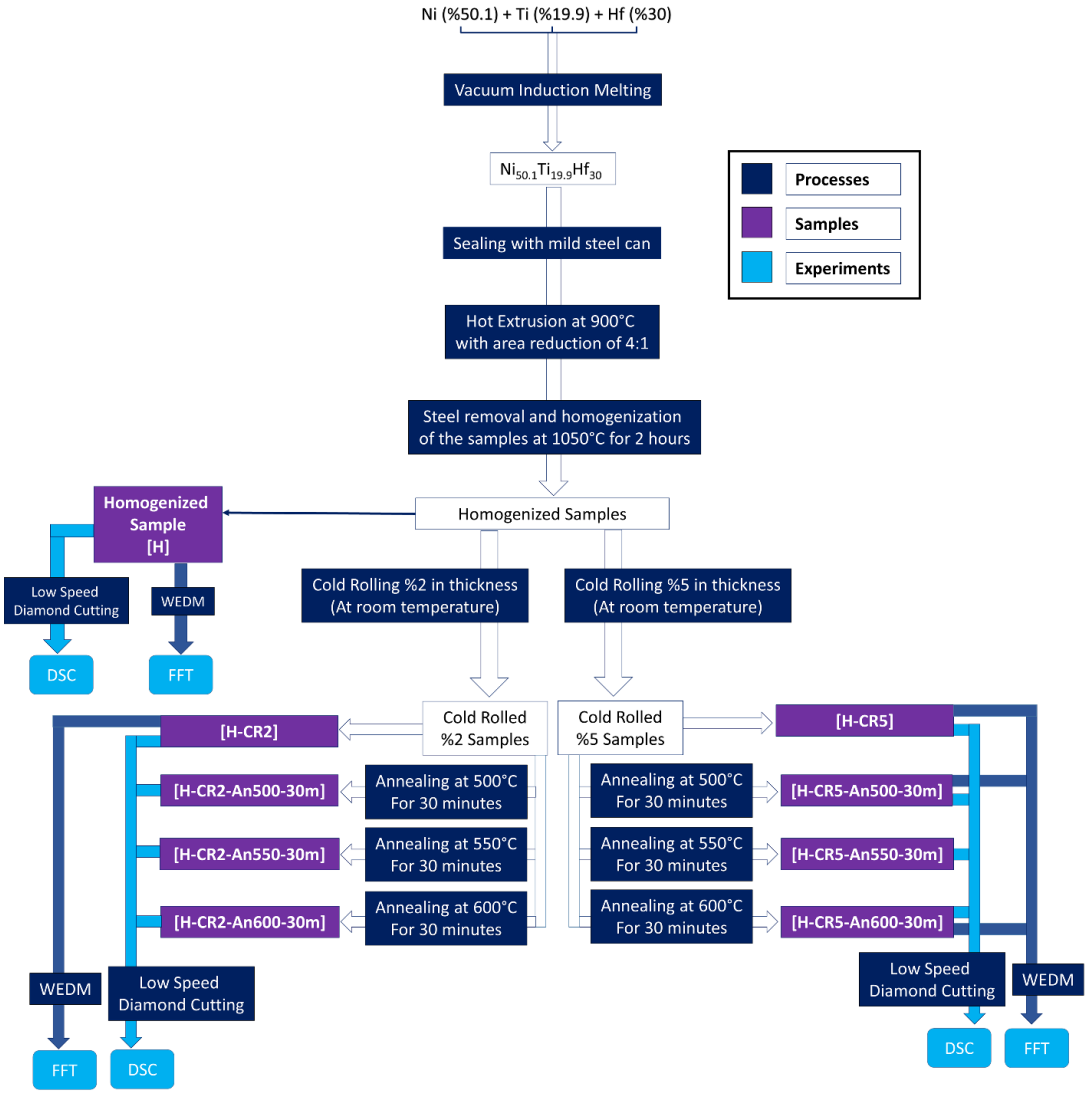

Figure 2.3-1. Sample processes and experiments that were done throughout the study.

3.1. As-Received Material

The $Ni_{50.1}Ti_{19.9}Hf_{30}$ (at%) SMA utilized in this work was produced by vacuum induction casting method. Quite pure elemental elements Ni, Ti, and Hf were melted and cast in a high purity argon environment. The material was then encased with mild steel to avoid friction and oxidation at the stage of hot extrusion shown in Figure 3.1-1, and then the billet was hot-extruded at 900 °C with a 4:1 area-reduction. Then steel was removed to cut samples for the experiments.

Figure 3.1-1. Hot Extruded $Ni_{50.1}Ti_{19.9}Hf_{30}$ (at%) alloy.

3.2. Homogenizing and Annealing Heat Treatments

Homogenization heat treatment is a technique in which the material is kept at a temperature below the solidus temperature of the alloys. It is highly beneficial in removing elemental segregation and texture formation, which may be inherited from casting and/or extrusion. Homogenization was conducted on all samples in a cylindrical furnace at 1050°C for 2 hours in this study. The reason for selecting a high temperature

and a short time for homogenization is due to the strong affinity of Hafnium to Oxygen. The time duration of the homogenization heat treatment was chosen as short as possible. For the same reason, samples were also covered by tantalum foil with a 25.4 μm thickness to avoid further oxidation and homogenized under a high purity argon atmosphere. All of the samples were homogenized in this study; therefore, letter "H" was used in the abbreviated names of the samples, as shown in Figure 2.3-1.

3.3. Cold Rolling and Annealing

The samples were cut into plate forms from the hot extruded $Ni_{50.1}Ti_{19.9}Hf_{30}$ (at%) billet using Wire Electrical Discharge Machine (WEDM). The plates were then rolled using a laboratory type rolling machine at room temperature. Some of the specimens have cold rolled by 2% and the others were cold rolled by 5% reduction in thickness. Since NiTiHf alloys are difficult to deform due to the Hafnium content, it was hard to achieve high thickness reduction without forming cracks. Before going further in the studies, cold-rolled samples were examined under optical microscope to control the possible crack formations. If surface cracks were determined after the cold rolling process and if they were shallow the samples were lightly grinded for the removal of these cracks. However, if it was not possible to remove them then the cold rolling was applied on a virgin WEDM cut plates. Nikon LV150 Optical Microscope was used to control the test specimens. In this manuscript, cold-rolled samples are indicated with the letters “CR” and the numbers corresponding to the reduction in thickness magnitude. (e.g., a sample that was homogenized and then cold-rolled by %5 is defined as H-CR5 as shown in Figure 2.3-1.)

Annealing was also done after cold rolling process to recover some of the undesired impacts of cold rolling on the FF properties of SMA. Some cold-rolled samples were annealed at 500 °C and 600 °C for 30 minutes to affirm the effect of annealing temperature on TTs, actuation strain, and irrecoverable strain and their stability throughout their fatigue life. In this study, annealed samples are defined according to their annealing temperature and time. (e.g., a sample that was annealed at 500 °C for 30 minutes is names as An500-30m as shown in Figure 2.3-1.

3.4. Sample Preparation

Homogenized, cold rolled as well as annealed samples were prepared for DSC experiments and Functional Fatigue Tests (FFT) in this study. DSC was utilized to determine the evolution of the TTs with the applied cold rolling and annealing processes. Samples used in the DSC experiments were considerably small and they were cut with a diamond saw cutter at a very low speed and without applying load to ensure no stress was induced to the samples since TTs should not change due to the cutting process. On the other hand, FFT samples were prepared via cutting into a specific shape called "dog bone", which is shown in Figure 3.4-1 by WEDM. WEDM is a cutting technique that helps to minimize the residual stresses that may be induced during conventional machining techniques.

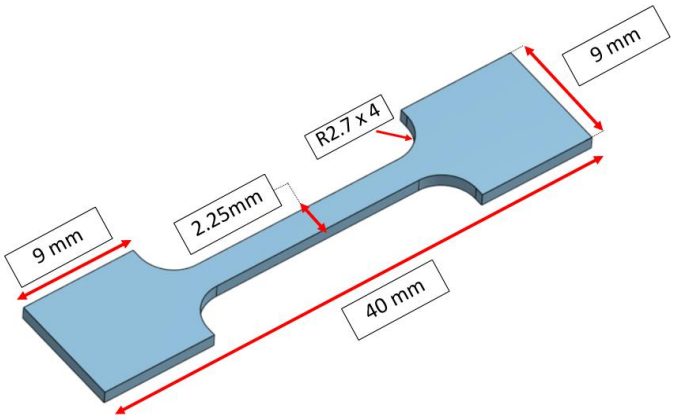

Figure 3.4-1. A dog-bone shaped sample used in Functional Fatigue Tests.

3.5. Differential Scanning Calorimetry (DSC)

The Differential Scanning Calorimetry (DSC) is a technique that measures the thermal energy collected or dissipated by a material over a period of time. This technique is used to determine some thermal and thermodynamic parameters such as transformation enthalpy, specific heat, and TTs [57]. In this study, the TTs of the samples were firstly examined by DSC (Perkin Elmer 8000) in stress-free conditions to understand the evolution of TTs with the applied mechanical and thermal treatments and to decide the UCT which was used in FFTs. Samples were cycled between 200 °C and 700 °C with a constant 10 °C/min heating-cooling rate. Sample preparation stages and processes are shown in Figure 2.3-1.

3.6. Functional Fatigue Experiments

A custom-built "functional fatigue test (FFT) machine" was used to evaluate $Ni_{50.1}Ti_{19.9}Hf_{30}$ (at%) alloy's FF behavior. The samples were heated by the Joule heating and cooled via natural convection. Dead weights were hung to apply the desired stress magnitude of 300MPa The schematic of the test set up as shown in Figure 3.6-1. During the experiment, an "Optris Ctlaser LTF-CF1 infrared thermometer" was used to detect the temperature from the middle of the samples' gage, and a "linear potentiometric displacement sensor" was used to measure the displacement. A DC power supply was utilized to heat the sample by passing a current through it, while the materials was cooled via natural convection as stated above. Lab View Software was used to manually enter the test parameters such as heating and cooling rate, UCT and LCT. Samples were heated at a rate of 15 °C/s and subjected to 300 MPa while they were kept at the austenite phase. Then, samples were cooled below their M_f temperatures and heated back above their A_f temperatures. The temperature and displacement data were automatically collected by using the National Instruments USB-6003 data logger [56].

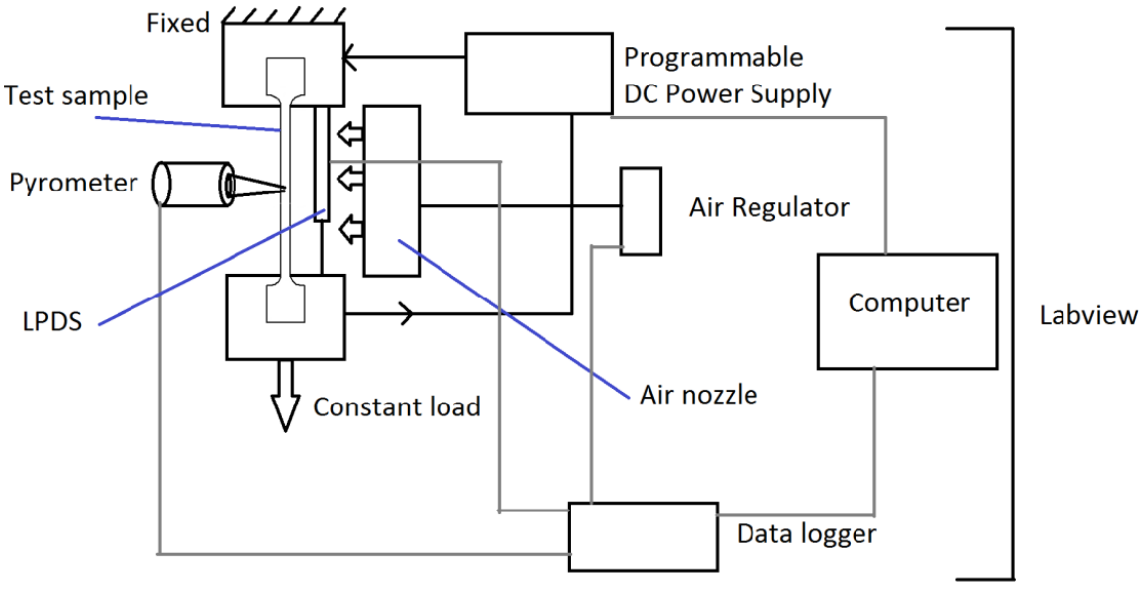

Figure 3.6-1. Illustration of FFT setup [56].

4. EXPERIMENTAL RESULTS

4.1. Differential Scanning Calorimetry (DSC)

DSC experiments were conducted on H, H-CR2, H-CR2-An500-30m, H-CR2-An550-30m, H-CR2-An600-30m, H-CR5, H-CR5-An500-30m, H-CR5-An550-30m, and H-CR5-An600-30m samples. TTs have obtained from the intersections of tangent lines as shown schematically in Figure 4.1-1.

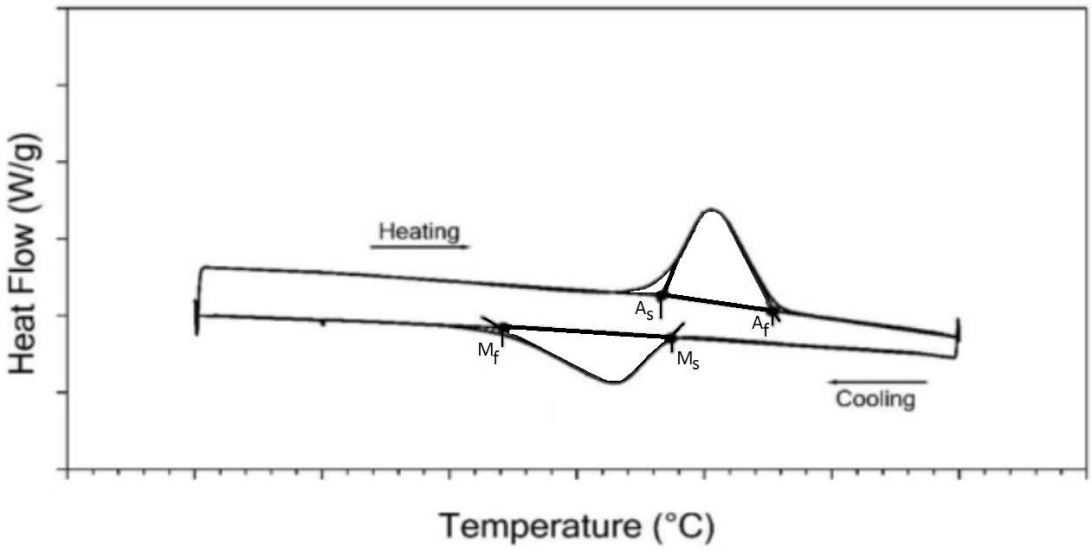

Figure 4.1-1. Application of tangent line method on the typical Heat Flow vs. Temperature curves gathered from DSC experiment results.

Results of the experiments are shown in Figure 4.1-2 and Figure 4.1-3. As an output of this experiment, heat flow vs. temperature data were gathered and the heating and cooling cycles are drawn separately for clear representation, as shown in Figure 4.1-2 and Figure 4.1-3.

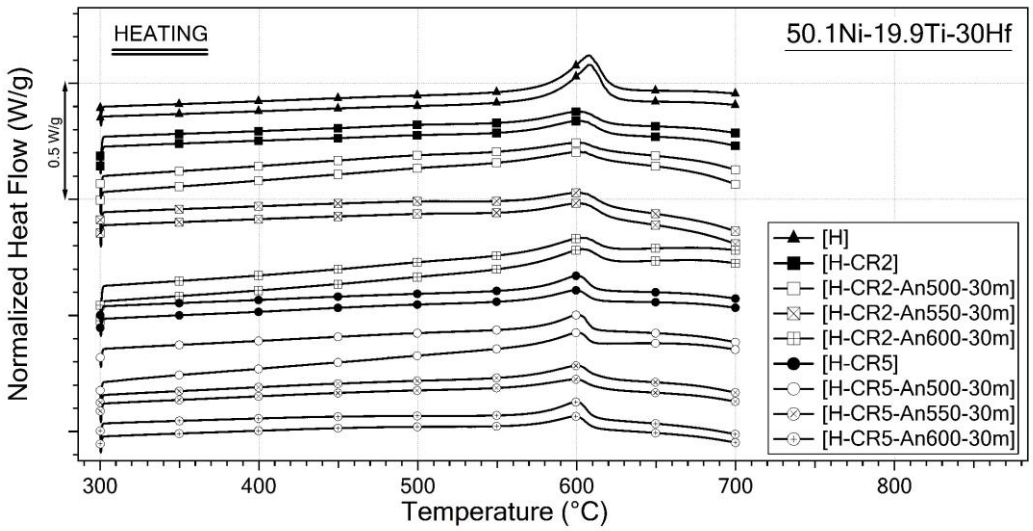

Figure 4.1-2 Heating curves of all samples obtained from DSC.

It is worth to note that that the areas under the transformation peaks in DSC curves provide the transformation enthalpy values. Cold-rolled samples demonstrated transformation peaks, which have smaller areas. Therefore, it can be stated that transformation enthalpies of cold rolled samples are relatively lower. As dislocation density increases, transforming volume decreases since dislocations act as barriers to austenite-martensite boundary, thus increasing the dislocation density may lead to suppression in phase transformation [5]. Moreover, M_f temperatures were roughly read from the DSC curves of the cold rolled samples since cooling curves were not sharp enough to apply tangent method as seen in Figure 4.1-3.

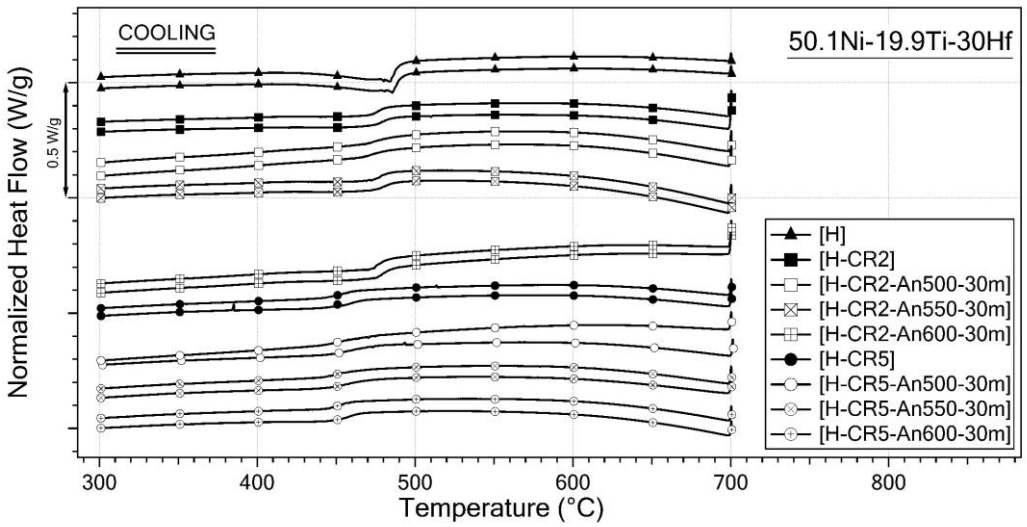

Figure 4.1-3. Cooling curves of all samples obtained from DSC.

TTs, which were drawn from heating and cooling curves in Figure 4.1-2 and Figure 4.1-3, are tabulated in Table 4.1-1. TTs were decreased via applying cold rolling due to an increase in dislocation density and possible grain size refinement. Increase in cold rolling percentage led to further decreases in TTs. For simplicity, all these analyses can be done by taking a close look at M_s temperature. Generally speaking, TTs were increased with the subsequent annealing heat treatments since annealing causes partial annihilation of dislocations and reduces dislocation density in the sample. It has been already known that the amount of dislocation annihilation increases as the annealing temperature rises. Therefore, it should be expected to observe a higher increase in TTs when the sample is annealed at higher temperatures. On the other hand, M_s temperatures decrease especially when the samples were annealed at 600°C and this might be due to ease of oxidation of NiTiHf at relatively higher temperatures. It can be deduced from this observation that the oxygen affinity of NiTiHf alloys further increase at 600°C and higher temperatures. The difference between the first and second cycles showed that TT stability does not change significantly in stress-free DSC experiments. In general, an increase in cold work helps stabilization of shape memory properties since an increase in dislocation density reduces plastic accommodation of the shape change. However, it important to recall that NiTiHf alloys with higher Hf content showed promising TT stability in DSC experiments as previously shown in the literature [38].

Table 4.1-1. TTs of all samples from DSC experiments.

Sample	Cycle	Transformation Temperatures (°C)			
		A_s	A_f	M_s	M_f
H	1	581	623	493	433
	2	579	625	492	432
	Difference (°C)	-2	2	-2	-1
H-CR2	1	566	623	486	425
	2	567	621	484	417
	Difference (°C)	2	-2	-3	-8
H-CR2-An500-30m	1	559	620	495	467
	2	559	619	491	465
	Difference (°C)	0	-1	-4	-1
H-CR2-An550-30m	1	562	622	490	473
	2	562	622	487	470
	Difference (°C)	0	0	-3	-3
H-CR2-An600-30m	1	570	622	487	476
	2	570	620	483	473
	Difference (°C)	1	-2	-5	-3
H-CR5	1	571	613	467	413
	2	565	614	460	414
	Difference (°C)	-6	1	-7	1
H-CR5-An500-30m	1	579	611	475	421
	2	574	610	475	422
	Difference (°C)	-5	-1	0	1
H-CR5-An550-30m	1	573	613	471	417
	2	570	613	465	416
	Difference (°C)	-3	0	-6	-1
H-CR5-An600-30m	1	573	611	467	393
	2	570	612	459	394
	Difference (°C)	-3	1	-8	1

4.2. Functional Fatigue Experiments

Functional fatigue tests (FFTs) were done by applying 300 MPa constant stress level on samples while heating and cooling. UCT was set to a temperature by being sure austenitic transformation was completed, while the lower cycle temperature (LCT) was set to achieve full and complete martensitic transformation. UCT and LCT were set by considering austenite finish and martensite finish temperatures, which were obtained from stress-free DSC experiment results. However, samples were heated to an UCT, which was approximately 100°C higher than that of A_f temperature obtained from DSC experiment since TTs increase with the applied stress and with the number of cycles during FFTs. 250 °C for LCT and 700 °C for UCT were chosen for all samples in FFTs.

It is also important to keep the same UCTs for all samples since it was shown in the literature that the transformation properties of HTSMAs is remarkably influenced by UCT [21].

The main concern of this study was to observe the influence of cold rolling and subsequent annealing processes on the FF properties such as evolution and stabilization of TTs, ε_{act} and T_{hys} during FF cycles. Therefore, considering the significant change of TT in DSC experiments by applying cold rolling and annealing, FFTs were conducted on H, H-CR2, H-CR5, H-CR5-An500-30m, and H-CR5-An600-30m samples since the effect of high and low percentage of cold rolling together with the annealing and relatively high temperature annealing on the FF properties of $Ni_{50.1}Ti_{19.9}Hf_{30}$ (at%) HTSMA was asked to compare. The procedure of determining the aforementioned FF properties was previously shown in Figure 2.1-2. It is worth to mention that all FFTs results were presented with strain-temperature responses and the fatigue properties were obtained from these curves.

The strain-temperature response of the homogenized (H) sample is shown in Figure 4.2-1. Some of the cycles are shown and some of them are removed from the figure for clear presentation. The FFT was conducted under 300 MPa and the fracture occurred at the 51st cycle.

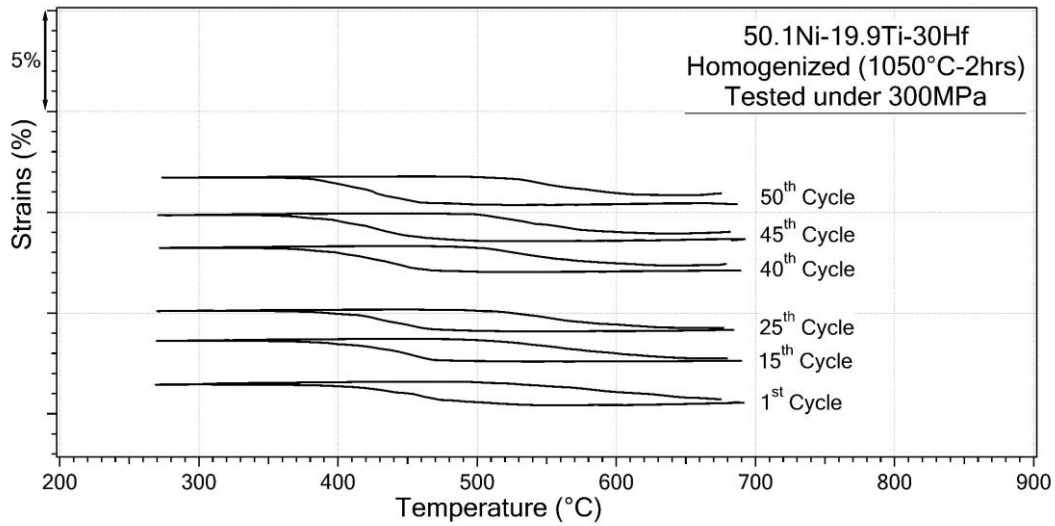

Figure 4.2-1. Strain-Temperature response of the homogenized (H) sample obtained from FFT.

The ε_{mar} and ε_{aus} values of the homogenized (H) sample were shown in Figure 4.2-2. ε_{aus}, in other words, total ε_{irr} was observed to increase relatively faster after 40th cycle.

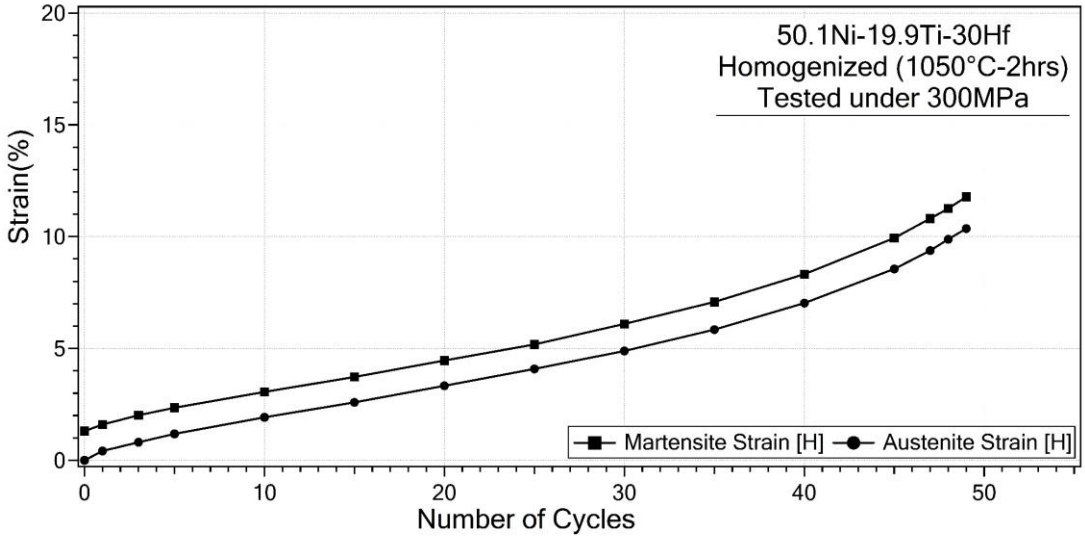

Figure 4.2-2. The evolution of the ε_{mar} and ε_{aus} of the homogenized (H) sample until the fracture.

The change in TTs of the homogenized (H) sample until the fracture is shown in Figure 4.2-3. It is observed that TTs did not change significantly until the fracture. Among all of the TTs, the change of A_f and M_s temperatures was relatively noticeable with the cycles. Numerical values of TTs with the cycles are also tabulated in Table 4.2-1. There is a decreasing tendency in all TTs as can be seen in Table 4.2-1 and this may be appertained to the dislocation formation during austenite-martensite phase transformation while heating-cooling. These dislocations hinder the austenite-martensite boundary motion. Therefore, more undercooling is necessary for martensitic transformation and more overheating is necessary for martensite to austenite transformation.

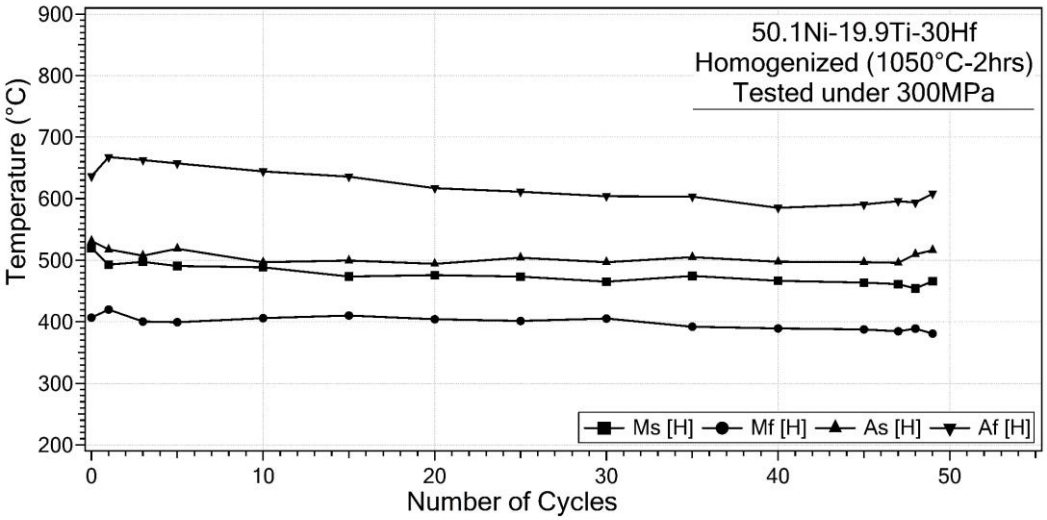

Figure 4.2-3. The change in TTs of the Homogenized (H) specimen over cycles.

Table 4.2-1. The change in TTs over cycles for the homogenized (H) sample.

Cycle	As (°C)	Af (°C)	Ms (°C)	Mf (°C)
1	531.3	636.3	519.6	406.9
2	517.4	667.7	493.0	419.9
4	507.5	662.9	497.5	400.5
6	518.6	657.3	490.7	399.3
11	496.8	644.4	488.6	406.0
16	499.7	635.7	473.6	410.3
21	494.3	617.0	475.9	404.2
26	504.2	611.3	473.5	401.5
31	496.8	604.0	465.2	405.3
36	505.1	603.3	474.6	392.1
41	497.7	585.1	466.7	389.4
46	497.0	590.7	463.7	387.8
48	495.9	595.9	461.3	384.6
49	509.7	593.8	454.4	388.9
50	516.2	608.1	466.0	380.9
Difference (°C) First and Last Cycles	15.0	28.2	53.6	26.0

The evolution of the ε_{act} of the homogenized (H) sample is shown in Figure 4.2-4. It is observed that ε_{act} values remained almost stable between 0.9 and 1.0%. There is a slight jump in the ε_{act} values gathered from the first and the second cycles, however, this can be explained with the first cycle effect. The residual stresses, which might be induced during cutting the test samples, are relieved in the heating stage of the first cycle. Thus, it is acceptable for the values in the 1st and 2nd cycles to be slightly different due to the release of the cutting induced stress.

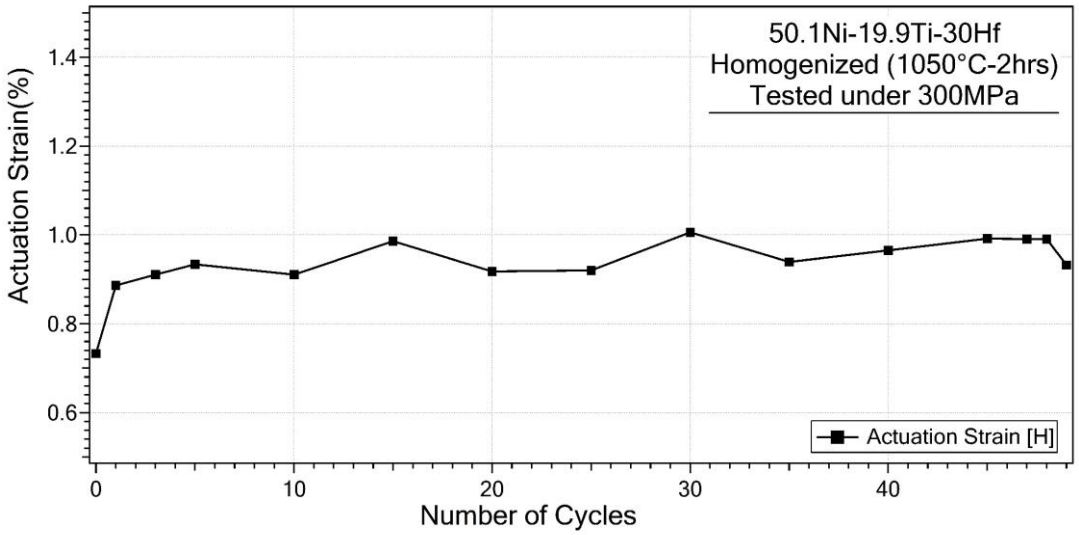

Figure 4.2-4. The change in ε_{act} of the homogenized (H) specimen until the fracture.

The change in the T_{hys} of the homogenized (H) specimen is shown in Figure 4.2-5. T_{hys} dropped from 170°C to 130°C during first 25 cycles then slightly increased after 45th cycle till the fracture.

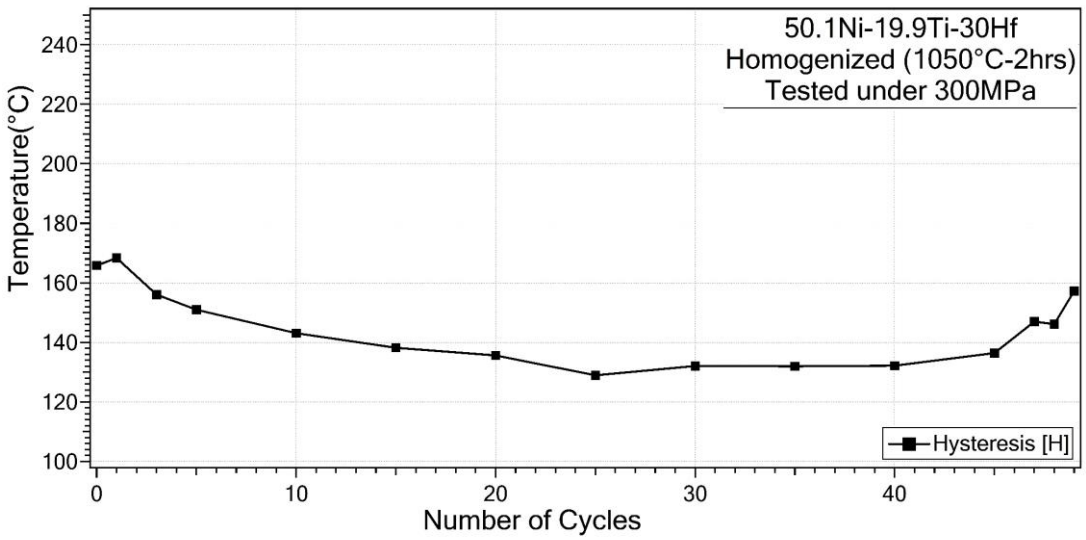

Figure 4.2-5. The T_{hys} evolution of the homogenized (H) sample.

The strain-temperature curves of the homogenized then cold-rolled %2 (H-CR2) sample are shown in Figure 4.2-6. Fracture was observed at the 38th cycle. The reason of observing early failure might be the crack formation in cold rolling operation. Although the cold rolling percentage was very low, crack formation was still observed since NiTiHf alloys with very high Hf content are known as hard to deform materials.

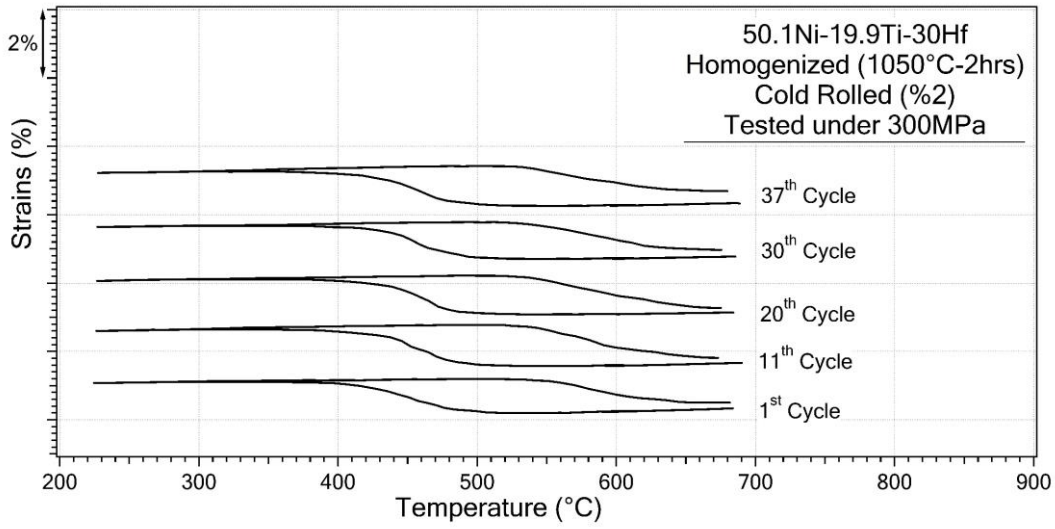

Figure 4.2-6. Strain-Temperature response of the H-CR2 sample obtained from FFT.

The ε_{mar} and ε_{aus} were obtained from strain-temperature curves and are shown in Figure 4.2-7. The ε_{aus} values, in other terms, the accumulated ε_{irr} values of H-CR2 sample were determined to be lower than that of homogenized, however, it should be noted that H-CR2 sample failed earlier than that of Homogenized sample.

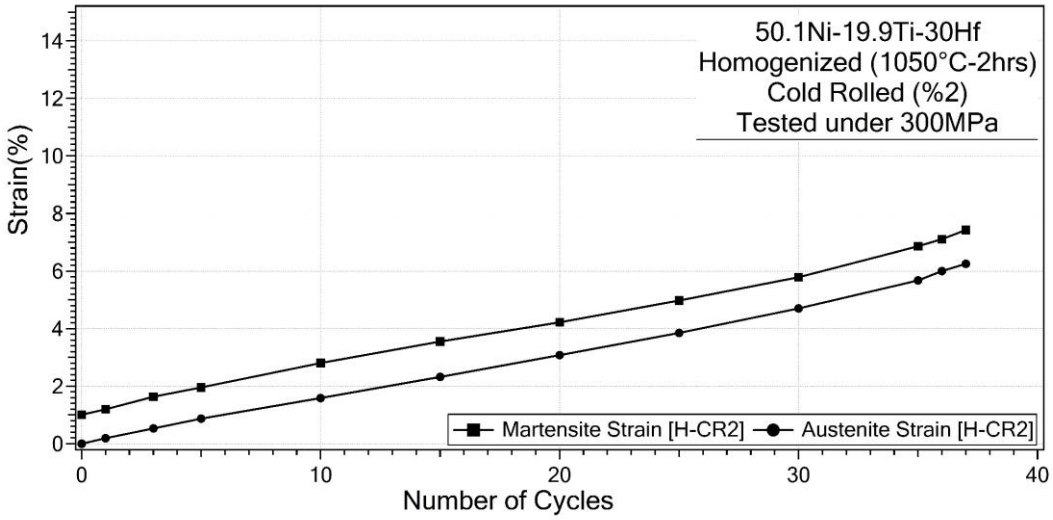

Figure 4.2-7. Evolution of the εmar and ε_{aus} of the H-CR2 sample until the fracture.

The change in TTs of H-CR2 sample until the fracture is shown in Figure 4.2-8. And TTs with the number of cycles are also tabulated in Table 4.2-2. It can be deduced from the Table 4.2-2 that the stability of TTs was improved after cold rolling due to the effect of rolling induced dislocations, which prevented further formation of dislocations during heating-cooling cycles [3]. The dislocation formation during the cycles leads to an instability in shape memory properties. However, if the SMAs are strengthened before running the cycles via applying cold rolling kind of deformation techniques, then dislocation formation during heating-cooling cycles mitigates.

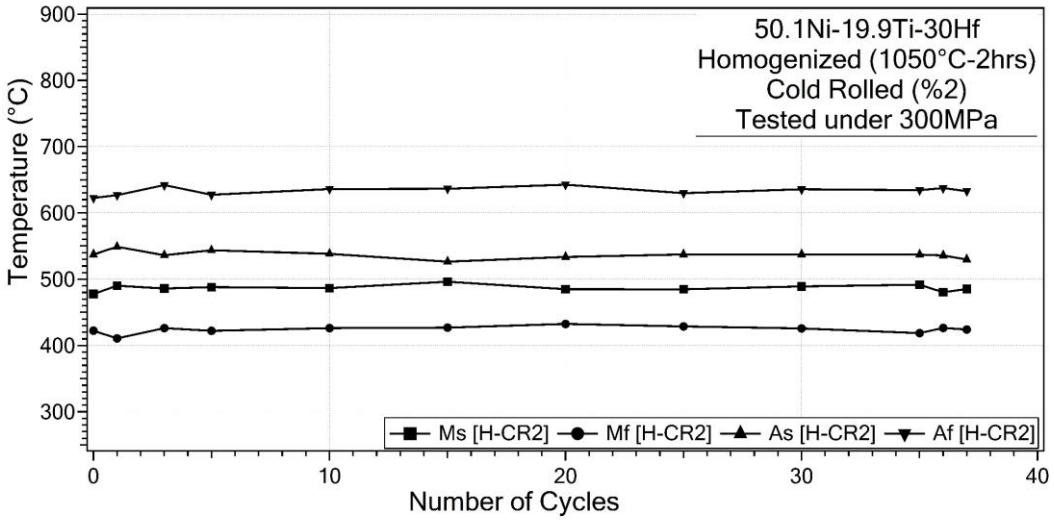

Figure 4.2-8. The change in TTs of the H-CR2 sample over cycles.

Table 4.2-2. The change in TTs over cycles for the H-CR2 sample.

Number of Cycles	As (°C)	Af (°C)	Ms (°C)	Mf (°C)
1	537.3	622.5	477.8	422.4
2	548.9	626.7	490.3	410.7
4	536.1	641.9	486.0	426.2
6	543.5	627.3	488.1	422.2
11	538.3	636.0	486.6	426.3
16	526.6	636.4	496.3	427.1
21	533.7	642.6	485.0	432.6
26	537.4	629.7	484.9	428.9
31	537.3	635.6	489.2	425.8
36	537.2	634.3	491.8	418.7
37	535.9	637.4	480.3	426.5
38	529.8	632.8	485.3	424.1
Difference (°C) First and Last Cycles	7.5	-10.4	-7.5	-1.7

The change in the ε_{act} of H-CR2 sample with the number of cycles is shown in Figure 4.2-9. It was observed that ε_{act} values increased until the 10^{th} cycle, remained almost stable

between the 10th and 25th cycles then started to decrease until the fracture. Actually, it was expected to observe stable ε_{act} values throughout the cycles. However, the stability was not attained. Additionally, the ε_{act} values of Homogenized and H-CR2 samples were found to be almost the same due to the fact that the cold rolling percentage was very low and not effective enough in changing the ε_{act} values.

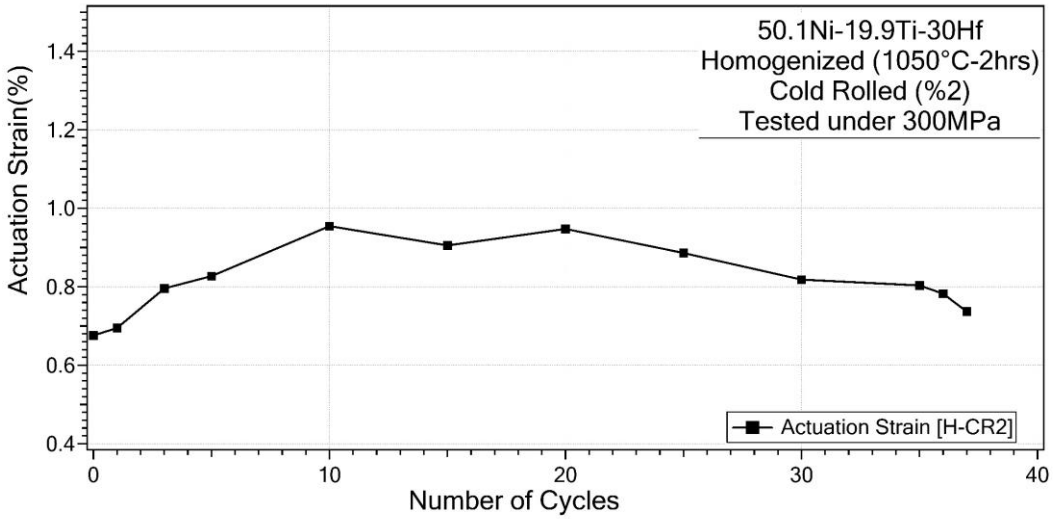

Figure 4.2-9. The change in ε_{act} of H-CR2 sample until the fracture.

The change in the T_{hys} of the H-CR2 specimen is shown in Figure 4.2-10. The evolution of T_{hys} of H-CR2 sample was observed to be the same as the evolution of T_{hys} of homogenized sample. T_{hys} dropped during the first 5 cycles and stayed almost stable until the last few cycles, then increased to initial values in the last cycles before fracture. Additionally, T_{hys} values of H-CR2 sample were higher than that of Homogenized sample, which can be appertained to the dislocation formation during rolling operation. Formation of T_{hys} is because of the internal friction, which impedes martensite-austenite boundary motion. Increase in dislocation density further increases the internal friction, so that the increase in T_{hys} was observed.

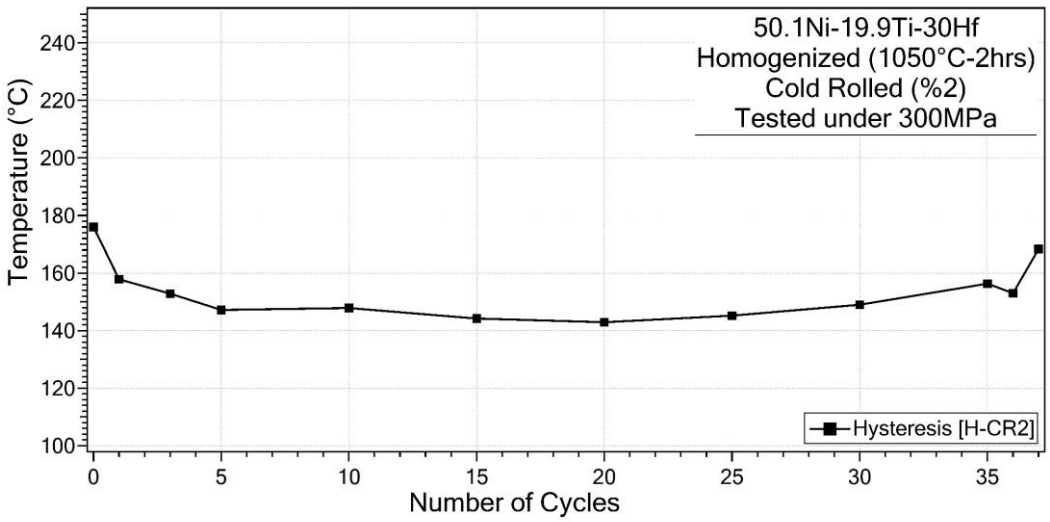

Figure 4.2-10. The T_{hys} evolution of the H-CR2 sample.

The strain-temperature curves of the homogenized and 5% cold-rolled (H-CR5) specimen are shown in Figure 4.2-11. The sample was failed at 46th cycle. It was observed that cold rolling has no positive effect on fatigue life of the alloy.

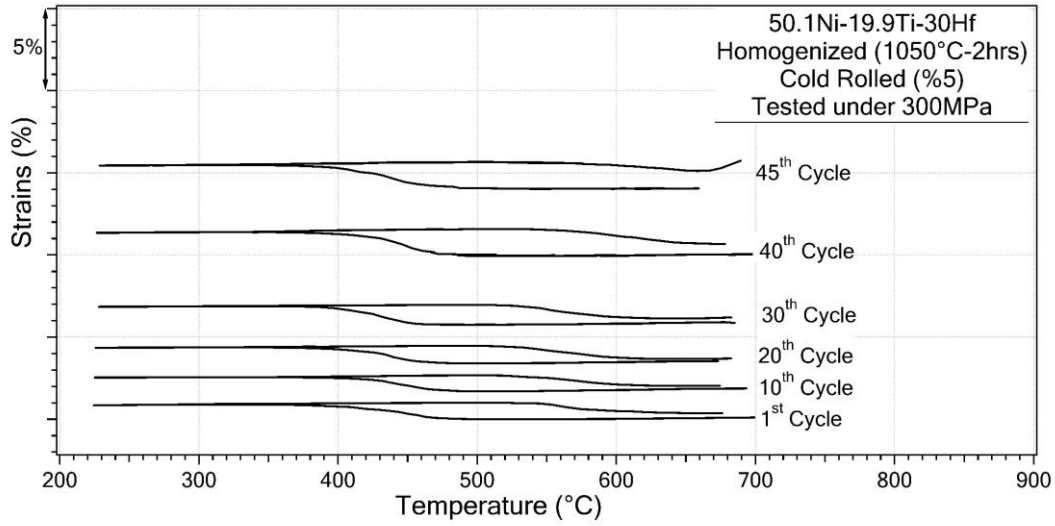

Figure 4.2-11. Strain-Temperature response of H-CR5 sample obtained from FFT.

The ε_{mar} and ε_{aus} from FFT of H-CR5 sample were gathered and are shown in Figure 4.2-12. The ε_{aus} increased faster after the 35th cycle. As the sample was close to fracture, the rate of increase in strain values increased and this might be due to the fact that the amount and the length of the cracks increased and this caused an increase in strain values with crack opening and closing.

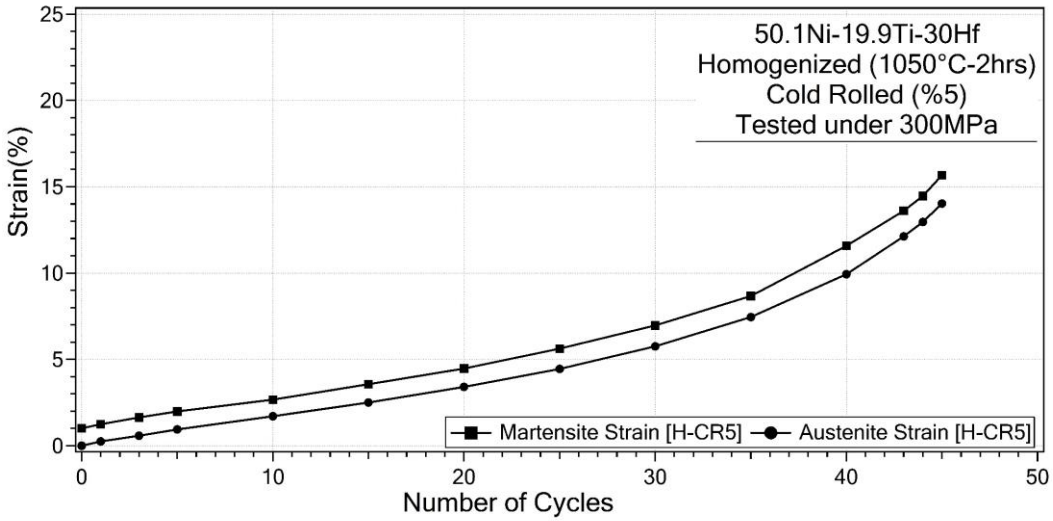

Figure 4.2-12. The evolution of the ε_{aus} and ε_{mar} until the fracture for the H-CR5 sample.

The change in TTs of the H-CR5 sample until the fracture is shown in Figure 4.2-13. It was observed that M_s and M_f did not change until the fracture and that A_s and A_f did not change noticeably until the 35th cycle, but then started to increase.

It can be seen that stability in TTs was improved after further increase in cold-rolling percentage because induced dislocations averted the formation of new dislocations in the matrix. A possible reason for A_s and A_f increase after the 35th cycle is the accumulation of cracks with the cycles. The discontinuities such as cracks may lead to attain residual stresses due to the stress concentrations at the crack tips; therefore, it is necessary to overheat the samples to higher temperatures for full austenitic transformation. Numerical results of TTs with the number of cycles are also tabulated in Table 4.2-3.

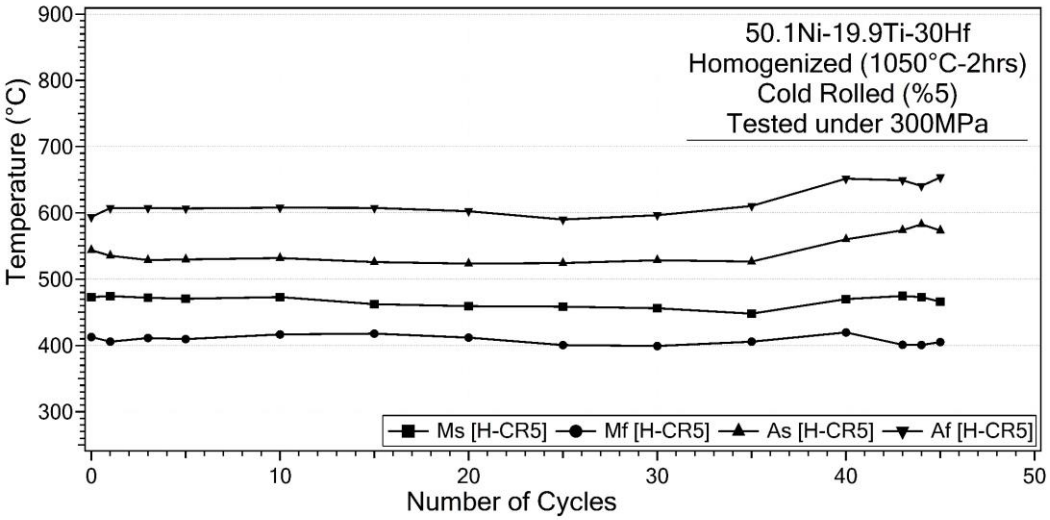

Figure 4.2-13. The change in TTs of the H-CR5 sample with the number of cycles.

Table 4.2-3. Transformation temperature change with the cycles for H-CR5 sample.

Number of Cycles	As (°C)	Af (°C)	Ms (°C)	Mf (°C)
1	543.6	593.7	473.1	412.8
2	535.5	607.4	474.7	405.8
4	529.0	607.4	472.1	411.3
6	529.9	606.8	470.6	409.7
11	532.1	607.9	473.1	416.7
16	526.0	607.4	462.4	417.9
21	523.6	602.5	459.4	411.9
26	524.5	590.0	458.6	400.7
31	528.7	596.4	456.2	399.3
36	526.7	610.5	448.1	405.7
41	560.1	651.6	470.1	419.7
44	573.7	649.3	474.7	401.1
45	582.8	640.6	473.1	400.7
46	573.5	653.6	466.0	405.2
Difference (°C) First and Last Cycles	-29.9	-59.9	7.1	7.6

The change in ε_{act} of the H-CR5 sample is shown in Figure 4.2-14. It was observed that ε_{act} values started to stabilize after the 15th cycle between 0.8 and 0.9%, then dropped sharply during the last couple of cycles. ε_{act} values were generally lower for the cold-rolled samples because a large number of induced dislocations by cold-rolling suppressed the martensite boundary movement, and transforming volume decreased [5]. In general, the deformation induced dislocations leads an increase in the critical shear stress for slip and hence, the cyclic stability of the shape memory properties of SMAs should be enhanced. However, as it is shown in Figure 4.2-14, the stability in ε_{act} was not achieved since crack formation and the internal stress due to rolling deformation increase with the increase in cold rolling percentage. Thus, the stress concentration regions around the crack tips and the internal stresses may cause the instability in ε_{act} values during FFT of H-CR5 sample.

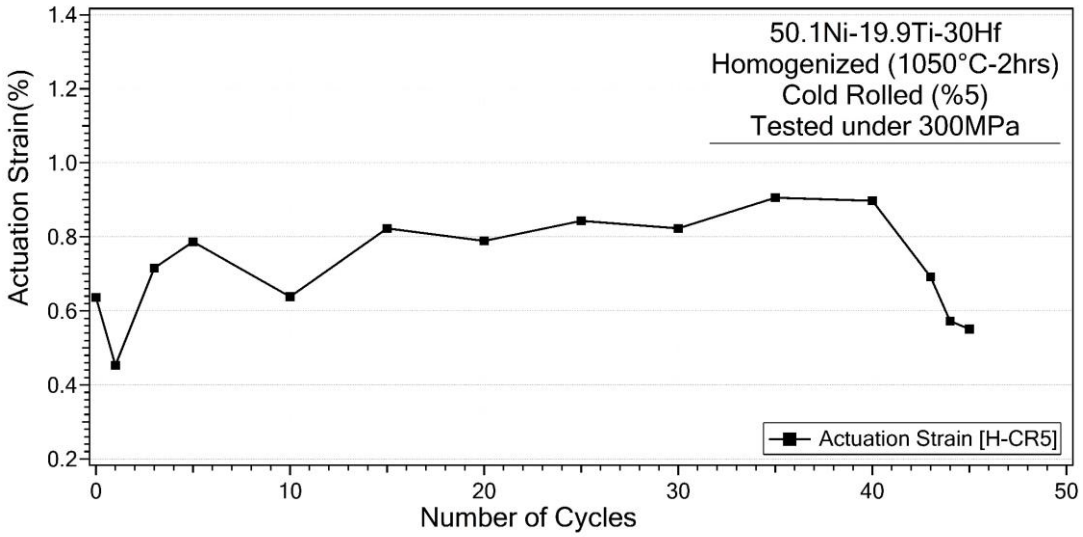

Figure 4.2-14. The change in ε_{act} of the H-CR5 sample until the fracture.

The change in the T_{hys} of the H-CR5 sample is shown in Figure 4.2-15. T_{hys} remained stable until the 35th cycle, then dramatically increased in the last few cycles before fracture due to the increase in austenitic transformation temperature.

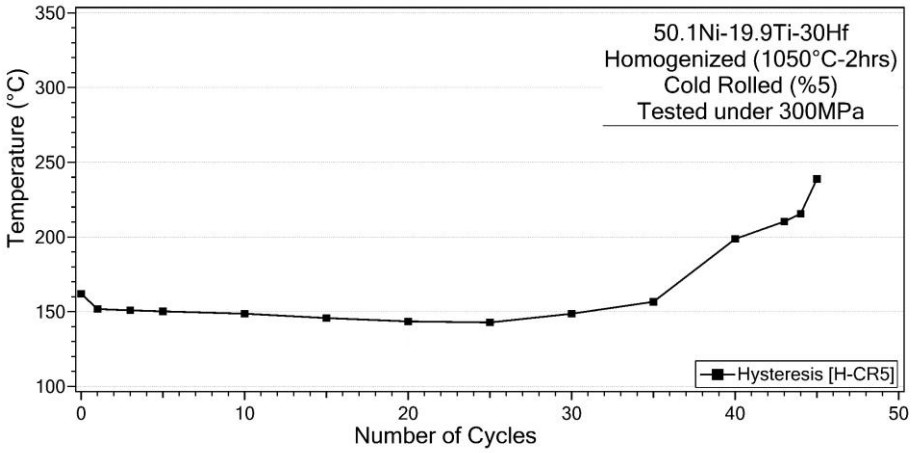

Figure 4.2-15. The T_{hys} evolution of the H-CR5 sample.

The strain-temperature response of the sample, which was first homogenized, then 5% cold-rolled and then annealed at 500 °C for 30 minutes, is shown in Figure 4.2-16. H-CR5-An500-30m coded sample was fractured at the 32nd cycle.

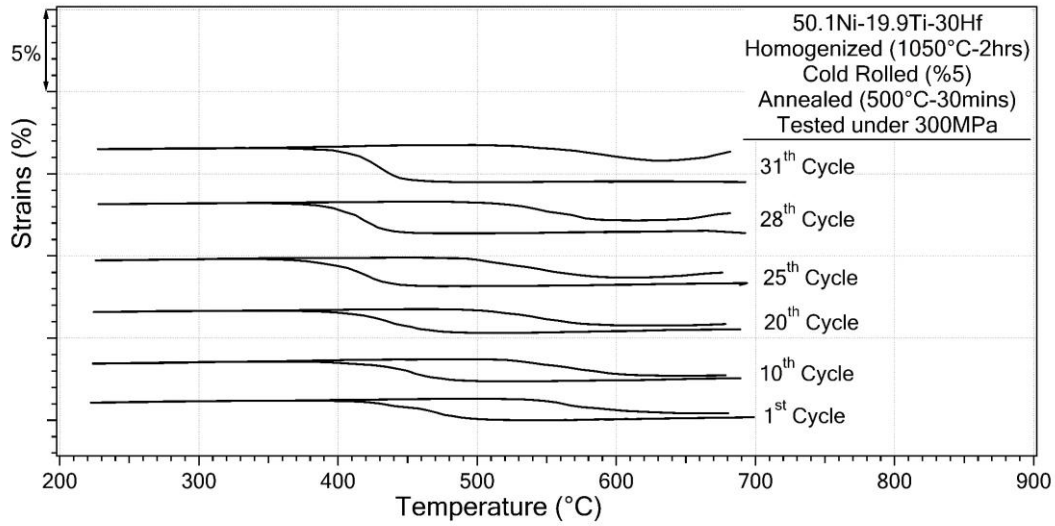

Figure 4.2-16. Strain-Temperature response of H-CR5-An500-30m sample obtained from FFT.

The ε_{mar} and ε_{aus} of H-CR5-An500-30m sample is shown in Figure 4.2-17. Strains increased sharply after the 25th cycle and continued to increase until the fracture.

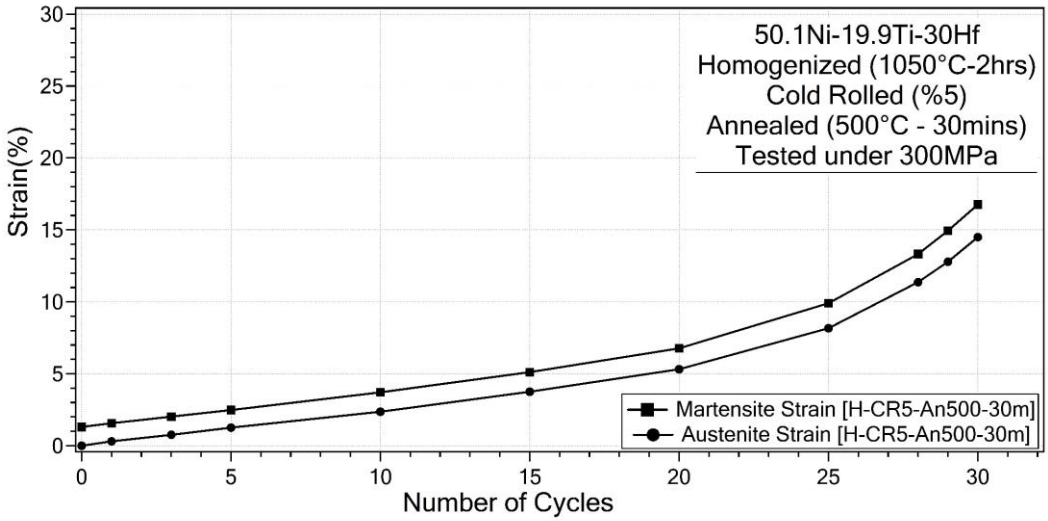

Figure 4.2-17. Evolution of the ε_{mar} and ε_{aus} of the H-CR5-An500-30m sample until the fracture.

The change in TTs of the H-CR5-An500-30m sample until the fracture is shown in Figure 4.2-18. TTs were found to be stable up to 27th cycle. An increase during last 2-3 cycles was realized. Annealing did not affect the stability of the TTs. Numerical results of TTs with the fatigue cycles are also tabulated in Table 4.2-4.

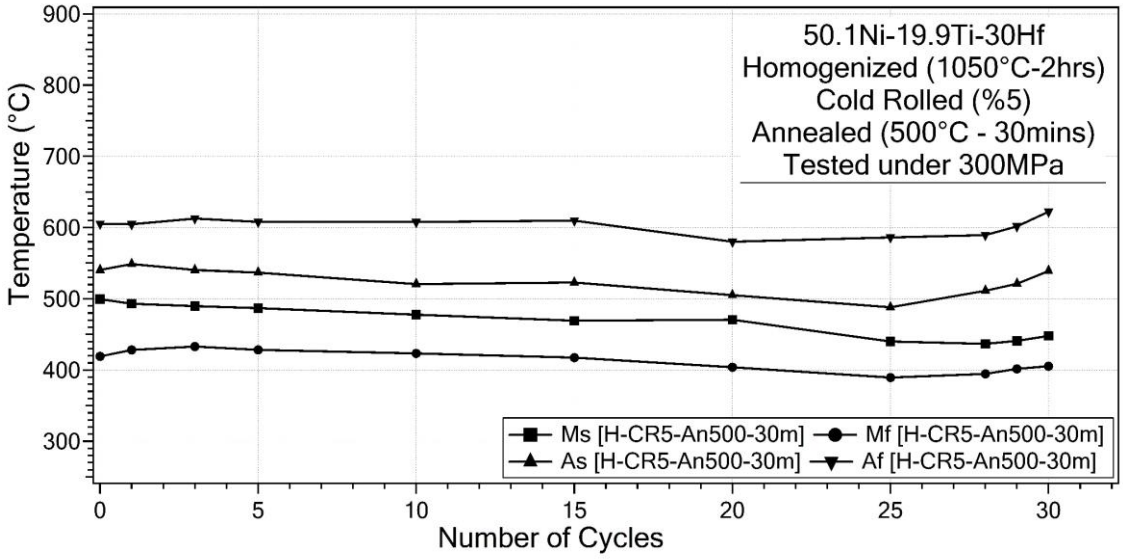

Figure 4.2-18. The change in TTs of the H-CR5-An500-30m sample over cycles.

Table 4.2-4. Transformation temperature change over cycles for H-CR5-An500-30m sample.

Number of Cycles	As (°C)	Af (°C)	Ms (°C)	Mf (°C)
1	540.4	605.2	499.6	419.2
2	548.7	604.5	493.2	428.1
4	540.4	612.6	489.8	433.1
6	536.9	607.9	487.0	428.4
11	520.7	607.8	477.7	423.4
16	523.0	609.8	469.3	417.5
21	505.2	580.0	470.7	403.9
26	488.2	586.1	440.0	389.6
29	511.3	589.4	436.7	394.6
30	521.1	601.6	441.0	401.7
31	539.1	622.2	448.0	405.5
Difference (°C) First and Last Cycles	1.3	-17.0	51.7	13.7

The change in the ε_{act} of H-CR5-An500-30m sample is shown in Figure 4.2-19. It was observed that ε_{act} values slightly increased until the 15th cycle, then slightly decreased and sharply increased until the 25th cycle, then finally decreased during the last five cycles.

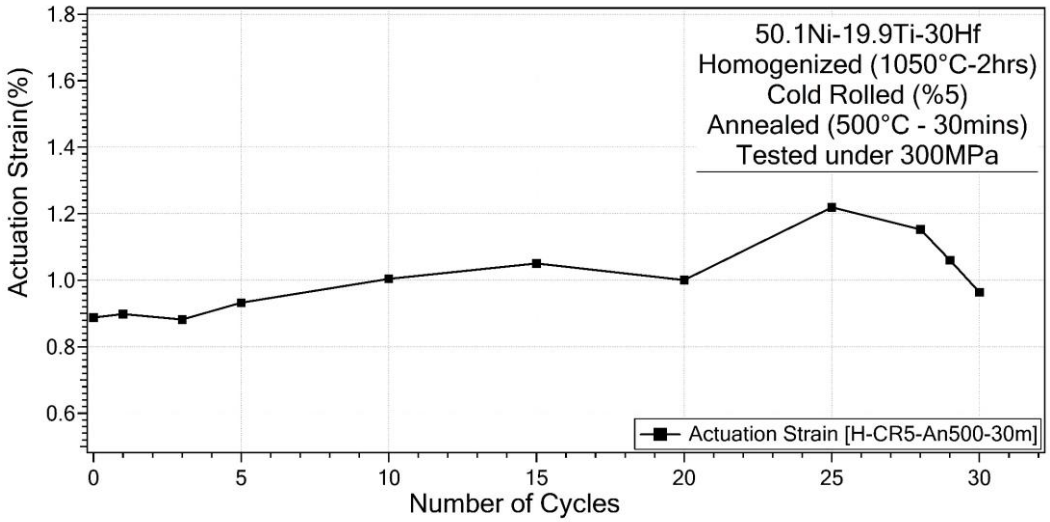

Figure 4.2-19. The change in ε_{act} of the H-CR5-An500-30m sample until the fracture.

The change in the T_{hys} of H-CR5-An500-30m coded sample is shown in Figure 4.2-20. T_{hys} remained stable until 20th cycle, then sharply increased during the last few cycles before the fracture.

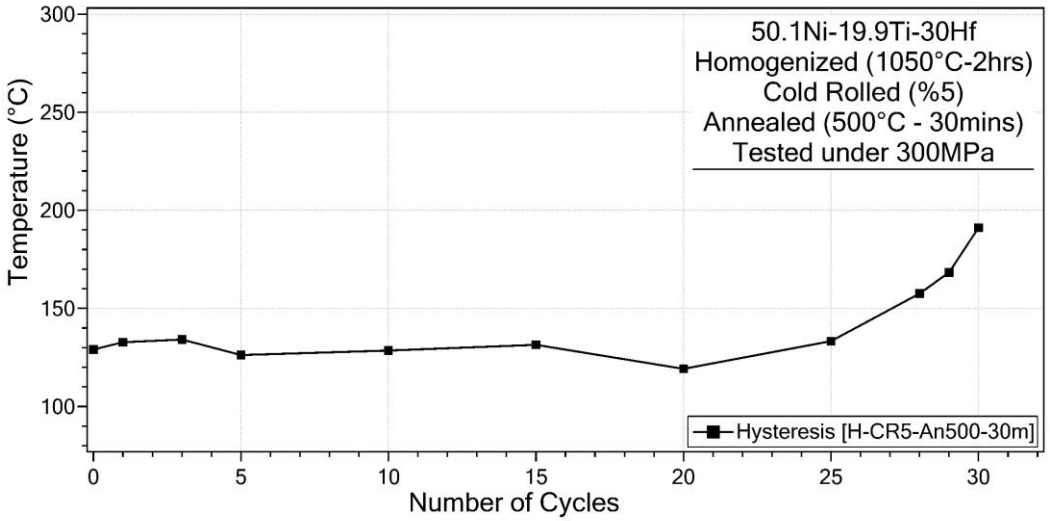

Figure 4.2-20. The T_{hys} evolution of the H-CR5-An500-30m sample.

The strain-temperature response of the sample, which was homogenized, 5% cold-rolled and then annealed at 600 °C for 30 minutes is shown in Figure 4.2-21. The fracture of H-CR5-An600-30m sample occurred at the 29th cycle.

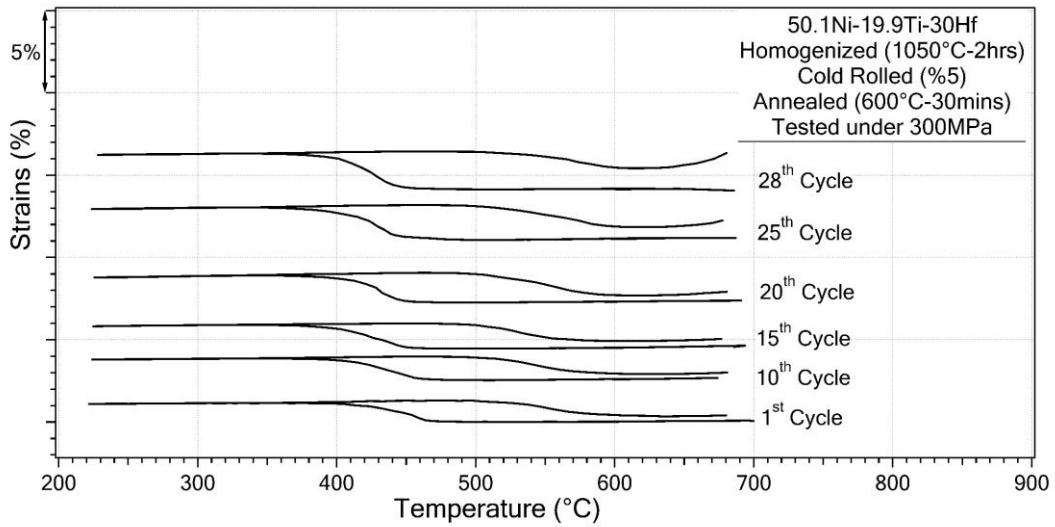

Figure 4.2-21. Strain-Temperature response of the H-CR5-An600-30m sample gathered from FFT.

The ε_{mar} and ε_{aus} of H-CR5-An600-30m were determined from strain-temperature curves and are shown in Figure 4.2-22. The ε_{aus} was observed to increase sharply after 20th cycle until the fracture.

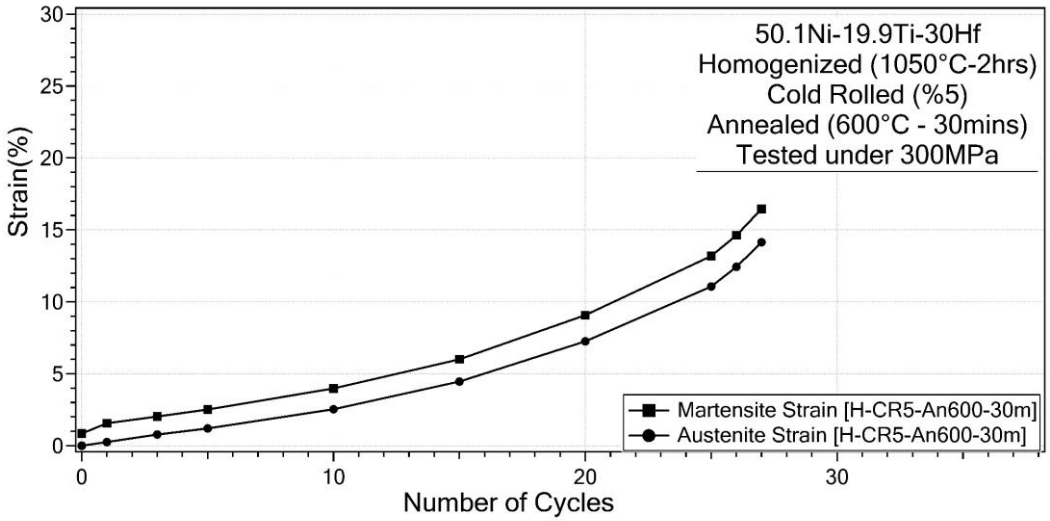

Figure 4.2-22. The evolution of the ε_{mar} and ε_{aus} of H-CR5-An600-30m sample until the fracture.

The change in TTs of H-CR5-An600-30m coded sample until the fracture is shown in Figure 4.2-23. It is promising to show that TTs remained almost constant until the fracture. Numerical results of TTs with the cycles are also tabulated in Table 4.2-5. However, it is worth to mention that the number of cycles, which was run on this sample, was very limited.

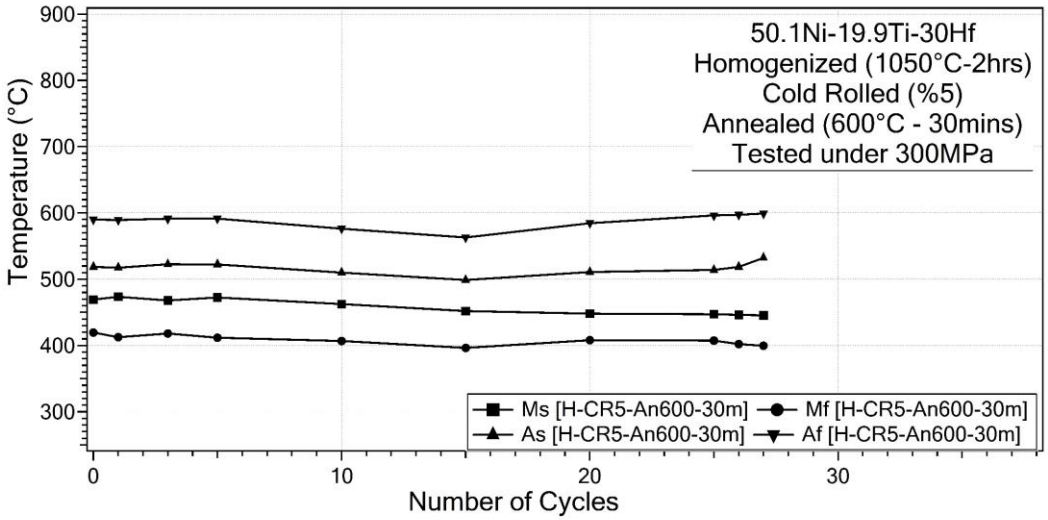

Figure 4.2-23. The change in TTs of the H-CR5-An600-30m sample over cycles.

Table 4.2-5. Transformation temperature change over cycles for H-CR5-An600-30m sample.

Number of Cycles	As (°C)	Af (°C)	Ms (°C)	Mf (°C)
1	518.6	589.9	469.3	419.7
2	517.3	589.3	473.5	412.6
4	522.7	591.1	468.0	418.2
6	522.3	591.4	472.5	411.7
11	510.0	576.2	462.5	406.9
16	498.9	562.9	452.1	396.4
21	510.9	584.4	448.0	408.0
26	514.0	596.1	447.2	407.5
27	518.6	597.1	446.2	402.1
28	532.3	599.1	445.5	399.5
Difference (°C) First and Last Cycles	-13.7	-9.1	23.8	20.2

The change in the ε_{act} values of H-CR5-An600-30m sample is shown in Figure 4.2-24. Except the noticeable ε_{act} difference between the first and second cycles, the values were similar for the first 15 cycles but then started to increase and then decrease. Similar behavior was also observed in H-CR5-An500-30m sample, as shown in Figure 4.2-19.

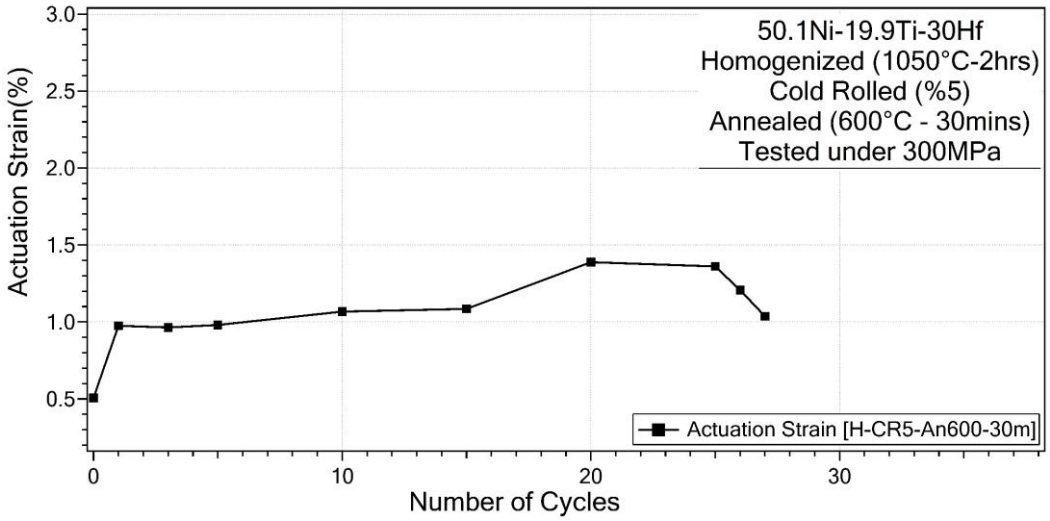

Figure 4.2-24. The change in ε_{act} of the H-CR5-An600-30m sample until the fracture.

The change in the T_{hys} of H-CR5-An600-30m sample is shown in Figure 4.2-25. T_{hys} remained stable until the 25th cycle, and then sharply increased in the last few cycles before fracture.

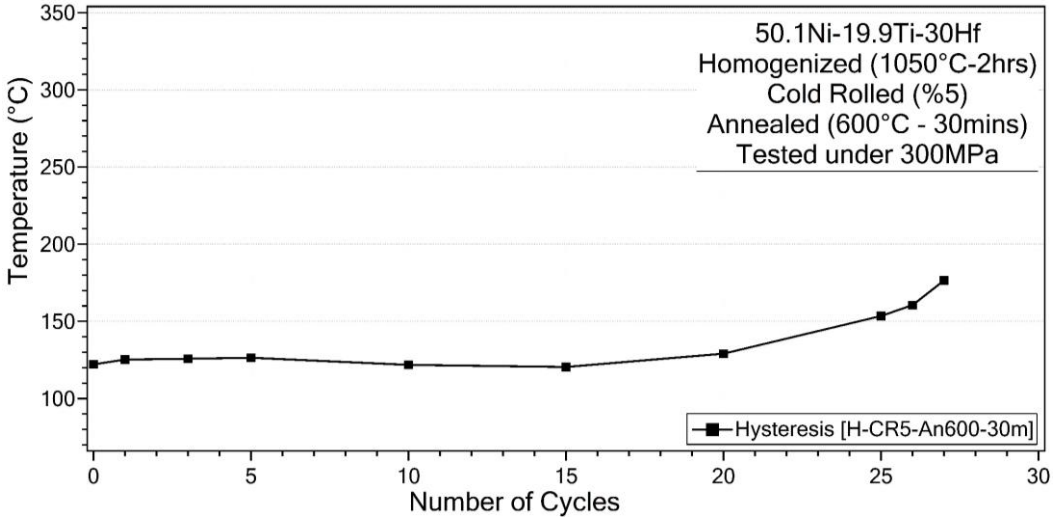

Figure 4.2-25. The T_{hys} evolution of the H-CR5-An600-30m sample.

To better understand the effect of cold rolling and subsequent annealing treatments, which were applied to the homogenized Ni50.1Ti19.9Hf30 (at%) HTSMA, the evolution of shape memory properties such as TTs, ε_{mar} and ε_{aus}, T_{hys} and ε_{act} of all samples with the number of cycles that were drawn from strain-temperature curves of FFTs were compared below.

For clear representation, just A_f and M_s temperatures of all samples were compared in Figure 4.2-26. First of all, by taking a look at Figure 4.2-26 one can easily see that A_f and M_s temperatures of H-CR2 and H-CR5 samples are lower than that of the homogenized sample since cold rolling led to a decrease in TTs due to martensite stabilization with the induced dislocations. The dislocations act as barriers to the martensite-austenite boundary, thus more overcooling is necessary to start martensitic transformation [50].

Additionally, A_f and M_s transformation temperatures of cold rolled samples stayed constant. On the other hand, the TTs of homogenized samples showed decreasing tendency throughout the FFT. Annealing had a slight effect on both stability and the evolution of the TTs. Since, annealing temperatures were kept relatively high but the time period for both of the annealing process was quite short. Therefore, the time might be only enough for rearrangement of dislocation forests and annihilation of excess dislocation and/or relieve of rolling induced internal stress.

Another intriguing observation was that annealing at higher temperature led a further decrease in TTs. This was not an expected result since the TTs rise with the increase in annealing temperature. There might be two reasons for the decrease in TTs with the increase in annealing temperature. The sample, which was annealed at 600°C and used in FFT might have more cracks that were formed during cold rolling process and the stress concentrations at the crack tips might one of the reasons in the decrease of the TTs. The other reason could be the oxidation of NiTiHf alloy at 600°C. It has been known that the oxygen affinity of these alloys is very high and actually increases with the increase in process temperatures. Thus, the reason of the decrease in TTs after annealing at 600°C might be the oxidation problem. To make sure for the decrease in TTs after 600°C annealing process, FFT can be repeated on a sample, which will be reprocessed via following cold rolling and subsequent annealing at 600 °C.

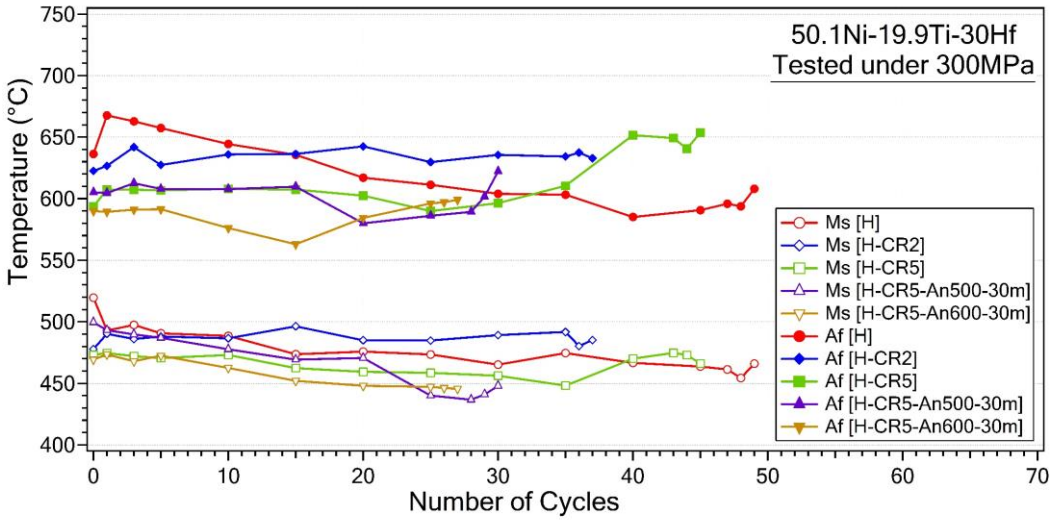

Figure 4.2-26. Comparison of the M_s and A_f temperatures with the number of cycles for the Samples H, H-CR2, H-CR5, H-CR5-An500-30m, and H-CR5-An600-30m.

The evolution of the ε_{mar} and ε_{aus}, which were determined from FFTs of all samples, is compared in Figure 4.2-27. As it can be seen that H and H-CR2 samples showed almost the same increasing trend in ε_{mar} and ε_{aus}. This was the main reason of investigating the cold rolling with subsequent annealing effect with FFTs only for cold-rolled 5% samples. It is worth to recall that; ε_{aus} value corresponds to the value of accumulated ε_{irr} that occurs at each cycle. It can be deduced from the figure that cold rolling caused an increase in ε_{aus} and ε_{mar} , and the subsequent annealing led to a further increase in the ε_{mar} and ε_{aus}. As mentioned before, NiTiHf HTSMAs with high Hf content are very hard to deform materials. In this study, NiTiHf alloy with 30at% of Hf was investigated and it was realized that application of cold rolling process on the aforementioned alloy was almost impossible. 2% and 5% of thickness reductions were hardly achieved in cold rolling processes. However, crack formations were determined after cold rolling processes using optical microscope. The surface cracks were removed via slight grinding of the samples; however, it was impossible to determine the possible inner cracks and to remove them. Cold rolling operations were repeated a couple of time when the detected surface cracks were deep. The microcracks, which was impossible to be determined, are the possible reasons for especially the increase in ε_{aus} because the stress concentration at the tip of the cracks can cause plastic deformation and lead to an increase in ε_{aus} . The increase in ε_{aus}, in other terms, the increase in accumulated ε_{irr} might be due to the dislocation induced plasticity at the crack tips that cause the formation of retained martensite. Additionally,

subsequent annealing after cold rolling led to a stress relieve in the matrix of the samples, therefore, the samples cannot resist to the crack propagation. As the crack propagation took place, the volume of the retained martensite further increased and led to observe higher ε_{irr} magnitudes in annealed samples.

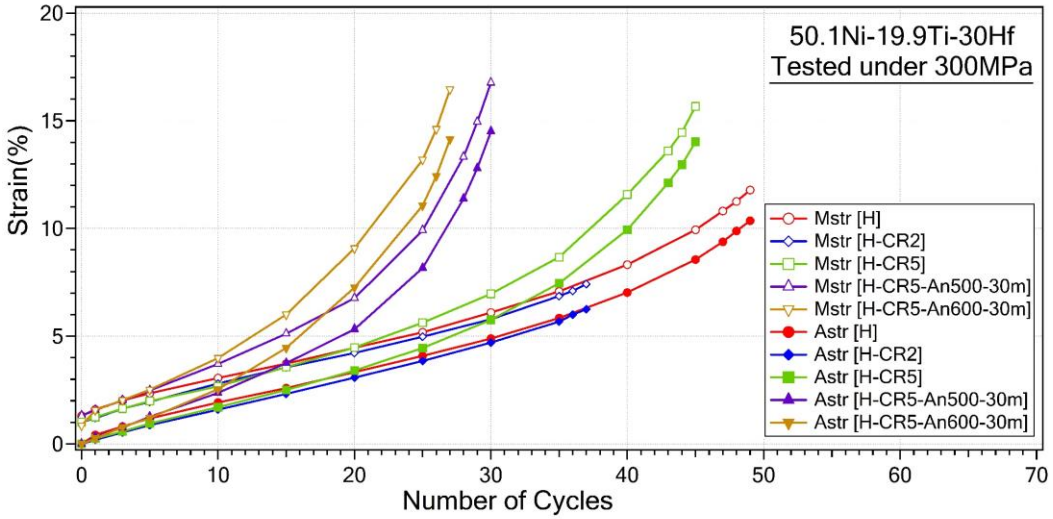

Figure 4.2-27. Comparison of the evolution of the ε_{mar} and ε_{aus} of H, H-CR2, H-CR5, H-CR5-An500-30m, and H-CR5-An600-30m samples.

The evolution of the ε_{act} of all samples is compared in Figure 4.2-28. As it can be seen, cold rolling has a reducing effect on ε_{act} due to the fact that cold rolling induces dislocations, which makes martensite-austenite phase boundary movement difficult and thus reduces the transforming volume. H-CR2, as mentioned before showed almost the same behavior as the homogenized sample because cold rolling 2% was not enough to see a change instead, induced micro cracks resulted in early failure of the specimen. Furthermore, the ε_{act} values increased with annealing because of the stress relieving and possibility of rearrangement of dislocation forests.

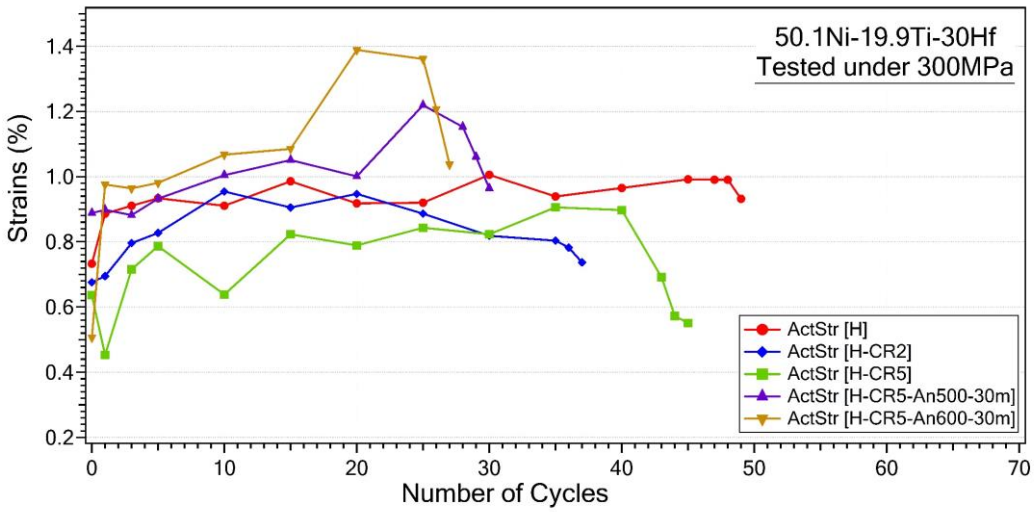

Figure 4.2-28. Comparison of the evolution of the ε_{act} of H, H-CR2, H-CR5, H-CR5-An500-30m, and H-CR5-An600-30m samples.

The evolution of the T_{hys} of all samples is compared in Figure 4.2-29. It has been already known that deformation processes generally increase and stabilizes the T_{hys} of SMAs. However, in this study, since the cold rolling percentages were kept low, the change in T_{hys} after cold rolling processes was not noticeable but the stability in the T_{hys} values was maintained at least until close to fracture.

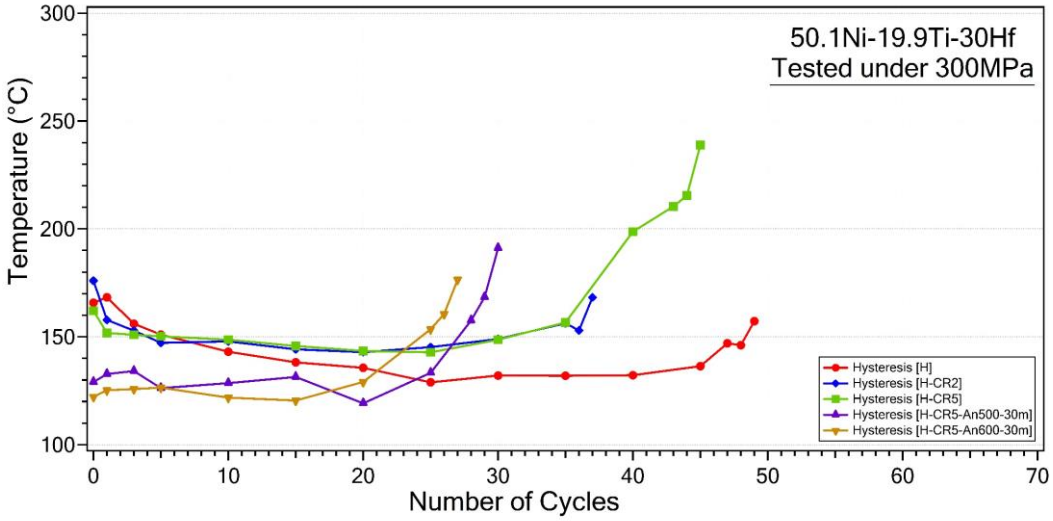

Figure 4.2-29. Comparison of the evolution of T_{hys} of H, H-CR2, H-CR5, H-CR5-An500-30m, and H-CR5-An600-30m samples.

5. CONCLUSION

Functional parameters of $Ni_{50.1}Ti_{19.9}Hf_{30}$ (at%) and the influence of cold-rolling with subsequent annealing were examined for the first time in the literature. These are the deduced outcomes from this study:

1) First of all, it is important to state that NiTiHf alloys are hard to deform materials. Since the hafnium content of $Ni_{50.1}Ti_{19.9}Hf_{30}$ (at%) alloy is very high it was very difficult to apply cold-rolling without causing any fracture or forming cracks. On the other hand, 30at% of Hf increased TTs of the alloy significantly, which made this research worth conducting. In the light of all this information, the effects of cold rolling with a small amount of reduction in thickness and the effects of subsequent annealing on the functional parameters of HTSMA under relatively high stress level of 300 MPa were studied in this work.

2) High atomic percentage of hafnium increased the TTs significantly and therefore, higher UCTs were set during FFTs. High magnitude of applied stress and high UCTs led to observe shorter fatigue lives and higher plastic deformation during heating-cooling cycles in FFTs for all samples with respect to the other NiTiHf alloys having lower TTs. This can be can be deduced from the observation of very high accumulated irrecoverable strains with less number of cycles.

3) The stabilization effect of the cold rolling and subsequent annealing was especially observed in TTs. Cold rolling led to observe stable TTs especially during first 30 cycles due to the possible dislocation formation.

4) Actuation strain values decreased with the cold rolling processes and then increased with the application of subsequent annealing. The decrease in actuation strain with cold rolling was due to the decrease in transforming volume. Generally speaking, the martensite-austenite boundary motion is inhibited with dislocations and thus the transforming volume decreases. Another possible reason for the decrease in actuation strain might be texture formation with the cold rolling. The texture, which was formed, may give the lower actuation strain. The later increase

in actuation strain with subsequent annealing was due to the annihilation of dislocations and/or rearrangement of dislocation forests.

5) Since the alloy used in this study was hard to deform due to its high hafnium content, micro-cracks probably formed inside of the samples. The surface cracks were controlled under the optical microscope before FFTs but the inner cracks were impossible to be determined. These cracks propagated during cycling and shortened the fatigue lives of the cold rolled samples. The maximum number of cycles before fracture was observed in the homogenized sample, which was 51 cycles.

Further studies should be performed via conducting Transmission Electron Microscope to control the microstructural evolution with the cold rolling and annealing processes. In this way, the formation of microcracks and dislocations can be detected and the FFT results can be better explained.

REFERENCES

[1] S. Seelecke and I. Mu¨ller, “Shape memory alloy actuators in smart structures: Modeling and simulation,” *Applied Mechanics Reviews*, vol. 57, no. 1, pp. 23–46, Jan. 2004.

[2] Y. Zhang, S. Jiang, L. Hu, and Y. Liang, “Deformation mechanism of NiTi shape memory alloy subjected to severe plastic deformation at low temperature,” *Materials Science and Engineering: A*, vol. 559, pp. 607–614, Jan. 2013.

[3] N. Babacan, J. Ma, O. S. Turkbas, I. Karaman, and B. Kockar, “The effects of cold rolling and the subsequent heat treatments on the shape memory and the superelasticity characteristics of Cu73Al16Mn11 shape memory alloy,” *Smart Materials and Structures*, vol. 27, no. 1, p. 015028, Dec. 2017.

[4] S. K. Wu, H. C. Lin, and Y. C. Yen, “A study on the wire drawing of TiNi shape memory alloys,” *Materials Science and Engineering: A*, vol. 215, no. 1–2, pp. 113–119, Sep. 1996.

[5] B. Kockar, I. Karaman, J. I. Kim, Y. I. Chumlyakov, J. Sharp, and C. J. (Mike) Yu, “Thermomechanical cyclic response of an ultrafine-grained NiTi shape memory alloy,” *Acta Materialia*, vol. 56, no. 14, pp. 3630–3646, Aug. 2008.

[6] T. Hoshiya, F. Takada, Y. Ichihashi, and H. R. Pak, “Restoration phenomena of neutron-irradiated Ti□Ni shape memory alloys,” *Materials Science and Engineering: A*, vol. 130, no. 2, pp. 185–191, Dec. 1990.

[7] G. B. KAUFFMAN and I. MAYO, “The Story of Nitinol: The Serendipitous Discovery of the Memory Metal and Its Applications,” *The Chemical Educator 1997 2:2*, vol. 2, no. 2, pp. 1–21, Jun. 1997.

[8] I. Khmelevskaya, E. Ryklina, and A. Korotitskiy, “Application of Thermomechanically Treated Ti-Ni SMA,” *Materials Science Foundations*, vol. 81–82, pp. 603–637, Mar. 2015.

[9] J. Seo, Y. C. Kim, and J. W. Hu, “Pilot study for investigating the cyclic behavior of slit damper systems with recentering shape memory alloy (SMA) bending bars used for seismic restrainers,” *Applied Sciences (Switzerland)*, vol. 5, no. 3, pp. 187–208, 2015.

[10] H. Holman, M. N. Kavarana, and T. K. Rajab, “Smart materials in cardiovascular implants: Shape memory alloys and shape memory polymers,” *Artificial Organs*, vol. 45, no. 5, pp. 454–463, May 2021.

[11] J. A. Balta, J. Simpson, V. Michaud, J. A. E. Månson, and J. Schrooten, “Embedded shape memory alloys confer aerodynamic profile adaptivity,” *Smart Materials Bulletin*, vol. 2001, no. 12, pp. 8–12, Dec. 2001.

[12] V. Brailovski, P. Terriault, T. Georges, and D. Coutu, “SMA actuators for morphing wings,” *Physics Procedia*, vol. 10, pp. 197–203, Jan. 2010.

[13] G.R Tomlinson and W.A Bullough, “Smart Materials and Structures: Proceedings of the 4th European and 2nd MIMR Conference,” 1998.

[14] S. C. Kwon, S. H. Jeon, and H. U. Oh, “Performance evaluation of spaceborne cryocooler micro-vibration isolation system employing pseudoelastic SMA mesh washer,” *Cryogenics (Guildf)*, vol. 67, pp. 19–27, Apr. 2015.

[15] B. Carpenter and J. Lyons, “EO-1 Technology Validation Report Lightweight Flexible Solar Array Experiment,” 2001.

[16] A. Johnson, “US5119555A - Non-explosive separation device,” 1990 Accessed: Jun. 02, 2022. [Online]. Available: https://patents.google.com/patent/US5119555A/en

[17] W. Abuzaid and H. Sehitoglu, “Functional fatigue of Ni50.3Ti25Hf24.7 – Heterogeneities and evolution of local transformation strains,” *Materials Science and Engineering: A*, vol. 696, pp. 482–492, Jun. 2017.

[18] G. Eggeler, E. Hornbogen, A. Yawny, A. Heckmann, and M. Wagner, “Structural and functional fatigue of NiTi shape memory alloys,” *Materials Science and Engineering: A*, vol. 378, no. 1–2, pp. 24–33, Jul. 2004.

[19] J. Frenzel, “On the Importance of Structural and Functional Fatigue in Shape Memory Technology,” *Shape Memory and Superelasticity*, vol. 6, no. 2, pp. 213–222, Jun. 2020.

[20] N. Babacan, K. C. Atli, O. S. Turkbas, I. Karaman, and B. Kockar, “The effect of dynamic aging on the cyclic stability of Cu73Al16Mn11 shape memory alloy,” *Materials Science and Engineering: A*, vol. 701, pp. 352–358, Jul. 2017.

[21] O. Karakoc *et al.*, “Effects of upper cycle temperature on the actuation fatigue response of NiTiHf high temperature shape memory alloys,” *Acta Materialia*, vol. 138, pp. 185–197, Oct. 2017.

[22] O. Karakoc, C. Hayrettin, D. Canadinc, and I. Karaman, “Role of applied stress level on the actuation fatigue behavior of NiTiHf high temperature shape memory alloys,” *Acta Materialia*, vol. 153, pp. 156–168, Jul. 2018.

[23] P. Conti, “Shape Memory and Superelasticity Announces New Additions to the Editorial Advisory Board,” *Shape Memory and Superelasticity 2018 4:1*, vol. 4, no. 1, pp. 264–265, Mar. 2018.

[24] C. M. Denowh and D. A. Miller, “Thermomechanical training and characterization of Ni–Ti–Hf and Ni–Ti–Hf–Cu high temperature shape memory alloys,” *Smart Materials and Structures*, vol. 21, no. 6, p. 065020, May 2012.

[25] M. J. Mahtabi, N. Shamsaei, and M. R. Mitchell, “Fatigue of Nitinol: The state-of-the-art and ongoing challenges,” *Journal of the Mechanical Behavior of Biomedical Materials*, vol. 50, pp. 228–254, Oct. 2015.

[26] W. Huang, “On the selection of shape memory alloys for actuators,” *Materials & Design*, vol. 23, no. 1, pp. 11–19, Feb. 2002.

[27] A. P. Lee, D. R. Ciarlo, P. A. Krulevitch, S. Lehew, J. Trevino, and M. A. Northrup, “A practical microgripper by fine alignment, eutectic bonding and SMA actuation,” *Sensors and Actuators A: Physical*, vol. 54, no. 1–3, pp. 755–759, Jun. 1996.

[28] W. Huang and W. Toh, “Training two-way shape memory alloy by reheat treatment,” *Journal of Materials Science Letters*, vol. 17, no. 19, pp. 1549–1550, 2000.

[29] T. Maruyama and H. Kubo, “Ferrous (Fe-based) shape memory alloys (SMAs): properties, processing and applications,” *Shape Memory and Superelastic Alloys*, pp. 141–159, Jan. 2011.

[30] R. Dasgupta, “A look into Cu-based shape memory alloys: Present scenario and future prospects,” *Journal of Materials Research*, vol. 29, no. 16, pp. 1681–1698, Aug. 2014.

[31] S. Miyazaki, T. Kawai, and K. Otsuka, “STUDY OF FRACTURE IN Cu-Al-Ni SHAPE MEMORY BICRYSTALS,” *Le Journal de Physique Colloques*, vol. 43, no. C4, pp. C4-813, Dec. 1982.

[32] J. Ma, I. Karaman, and R. D. Noebe, “High temperature shape memory alloys,” vol. 55, no. 5, pp. 257–315, Sep. 2013.

[33] J. van Humbeeck, “High Temperature Shape Memory Alloys,” *Journal of Engineering Materials and Technology*, vol. 121, no. 1, pp. 98–101, Jan. 1999.

[34] B.KOCKAR, “Shape memory behavior of ultrafine grained NiTi and TiNiPd shape memory alloys,” Doctoral thesis, Texas A&M University, 2007. Accessed: Jun. 02, 2022. [Online]. Available: https://oaktrust.library.tamu.edu/handle/1969.1/ETD-TAMU-2543

[35] H. E. Karaca *et al.*, “Effects of nanoprecipitation on the shape memory and material properties of an Ni-rich NiTiHf high temperature shape memory alloy,” *Acta Materialia*, vol. 61, no. 19, pp. 7422–7431, Nov. 2013.

[36] A. Manca, A. v. Shelyakov, and G. Airoldi, “Ageing in Parent Phase and Martensite Stabilization in a Ni50Ti30Hf20 Alloy,” *MATERIALS TRANSACTIONS*, vol. 44, no. 6, pp. 1219–1224, 2003.

[37] S. M. Saghaian *et al.*, “Effects of Ni content on the shape memory properties and microstructure of Ni-rich NiTi-20Hf alloys,” *Smart Materials and Structures*, vol. 25, no. 9, p. 095029, Aug. 2016.

[38] B. Kockar, I. Karaman, J. I. Kim, and Y. Chumlyakov, “A method to enhance cyclic reversibility of NiTiHf high temperature shape memory alloys,” *Scripta Materialia*, vol. 54, no. 12, pp. 2203–2208, Jun. 2006.

[39] P. E. Thoma and J. J. Boehm, “Effect of composition on the amount of second phase and transformation temperatures of NixTi90−xHf10 shape memory alloys,” *Materials Science and Engineering: A*, vol. 273–275, pp. 385–389, Dec. 1999.

[40] H. E. Karaca, E. Acar, H. Tobe, and S. M. Saghaian, “NiTiHf-based shape memory alloys,” vol. 30, no. 13, pp. 1530–1544, Nov. 2014.

[41] B. Kockar, I. Karaman, J. I. Kim, and Y. Chumlyakov, “A method to enhance cyclic reversibility of NiTiHf high temperature shape memory alloys,” *Scripta Materialia*, vol. 54, no. 12, pp. 2203–2208, Jun. 2006.

[42] S. Jiang, Y. Zhang, L. Zhao, and Y. Zheng, “Influence of annealing on NiTi shape memory alloy subjected to severe plastic deformation,” *Intermetallics (Barking)*, vol. 32, pp. 344–351, Jan. 2013.

[43] H. Morawiec, D. Stróz, and D. Chrobak, “Effect of Deformation and Thermal Treatment of NiTi Alloy on Transition Sequence,” *Le Journal de Physique IV*, vol. 05, no. C2, pp. C2-205, Feb. 1995.

[44] K. Adachi and J. Perkins, “Deformation of martensite in a polycrystalline Cu-Zn-AI alloy,” *Metallurgical Transactions A 1986 17:6*, vol. 17, no. 6, pp. 945–959, Jun. 1986.

[45] M. Pattabi and M. S. Murari, “Effect of Cold Rolling on Phase Transformation Temperatures of NiTi Shape Memory Alloy,” *Journal of Materials Engineering and Performance*, vol. 24, no. 2, pp. 556–564, Feb. 2015.

[46] T. Waitz, V. Kazykhanov, and H. P. Karnthaler, “Martensitic phase transformations in nanocrystalline NiTi studied by TEM,” *Acta Materialia*, vol. 52, no. 1, pp. 137–147, Jan. 2004.

[47] Q. S. Mei, L. Zhang, K. Tsuchiya, H. Gao, T. Ohmura, and K. Tsuzaki, “Grain size dependence of the elastic modulus in nanostructured NiTi,” *Scripta Materialia*, vol. 63, no. 10, pp. 977–980, Nov. 2010.

[48] B. Kockar *et al.*, “Role of severe plastic deformation on the cyclic reversibility of a Ti50.3Ni33.7Pd16 high temperature shape memory alloy,” *Acta Materialia*, vol. 58, no. 19, pp. 6411–6420, Nov. 2010.

[49] W. D. Callister, *An introduction to materials science and engineering*, vol. 7th Edition. Wiley, 2007.

[50] N. Babacan, J. Ma, O. S. Turkbas, I. Karaman, and B. Kockar, “The effects of cold rolling and the subsequent heat treatments on the shape memory and the superelasticity characteristics of Cu73Al16Mn11 shape memory alloy,” *Smart Materials and Structures*, vol. 27, no. 1, p. 015028, Dec. 2017.

[51] C. M. Denowh and D. A. Miller, “Thermomechanical training and characterization of Ni–Ti–Hf and Ni–Ti–Hf–Cu high temperature shape memory alloys,” *Smart Materials and Structures*, vol. 21, no. 6, p. 065020, May 2012.

[52] D. C. Lagoudas, D. A. Miller, L. Rong, and P. K. Kumar, “Thermomechanical fatigue of shape memory alloys,” *Smart Materials and Structures*, vol. 18, no. 8, p. 085021, Jul. 2009.

[53] L. J. Meng, Y. Li, X. Q. Zhao, and H. bin Xu, “Effects of Annealing on Phase Transformation and Mechanical Behaviors of NiTi Shape Memory Alloy Ultra Thin Sheet,” *Materials Science Forum*, vol. 546–549, pp. 2257–2260, May 2007.

[54] J. Gubicza, P. H. R. Pereira, G. Kapoor, Y. Huang, S. S. Vadlamani, and T. G. Langdon, “Annealing-Induced Hardening in Ultrafine-Grained Ni–Mo Alloys,” *Advanced Engineering Materials*, vol. 20, no. 9, p. 1800184, Sep. 2018.

[55] A. Evirgen, F. Basner, I. Karaman, R. D. Noebe, J. Pons, and R. Santamarta, “EFFECT OF AGING ON THE MARTENSITIC TRANSFORMATION CHARACTERISTICS OF A Ni-RICH NiTiHf HIGH TEMPERATURE SHAPE MEMORY ALLOY,” vol. 5, no. 4, Dec. 2012.

[56] H.Saygili, “The Development Of A Fatıgue Test Machine To Investigate The Functional Fatigue Life Of High Temperature Shape Memory Alloys And The Determination Of The Functional Fatıgue Life Of These Alloys,” Master Thesis, Hacettepe University, 2008.

[57] J. C. Zhao, “Methods for Phase Diagram Determination,” *Methods for Phase Diagram Determination*, 2007.